JACS
JOURNAL OF THE AMERICAN CHEMICAL SOCIETY

Article

pubs.acs.org/JACS

Selective Photochemistry at Stereogenic Metal and Ligand Centers of *cis*-[Ru(diphosphine)$_2$(H)$_2$]: Preparative, NMR, Solid State, and Laser Flash Studies

Marius V. Câmpian, Robin N. Perutz,* Barbara Procacci, Robert J. Thatcher, Olga Torres, and Adrian C. Whitwood

Department of Chemistry, University of York, York YO10 5DD, U.K.

Supporting Information

ABSTRACT: Three ruthenium complexes Λ-[*cis*-Ru((*R*,*R*)-Me-BPE)$_2$(H)$_2$] Λ-*R*,*R*-Ru1H$_2$, Δ-[*cis*-Ru((*S*,*S*)-Me-DuPHOS)$_2$-(H)$_2$] Δ-*S*,*S*-Ru2H$_2$, and Λ-[*cis*-Ru((*R*,*R*)-Me-DuPHOS)$_2$(H)$_2$] Λ-*R*,*R*-Ru2H$_2$ (**1** = (Me-BPE)$_2$, **2** = (Me-DuPHOS)$_2$) were characterized by multinuclear NMR and CD spectroscopy in solution and by X-ray crystallography. The chiral ligands allow the full control of stereochemistry and enable mechanistic studies not otherwise available. Oxidative addition of E−H bonds (E = H, B, Si, C) was studied by steady state and laser flash photolysis in the presence of substrates. Steady state photolysis shows formation of single products with one stereoisomer. Solid state structures and circular dichroism spectra reveal a change in configuration at ruthenium for some Δ-*S*,*S*-Ru2H$_2$/Λ-*R*,*R*-Ru2H$_2$ photoproducts from Λ to Δ (or vice versa) while the configuration for Λ-*R*,*R*-Ru1H$_2$ products remains unchanged as Λ. The X-ray structure of silyl hydride photoproducts suggests a residual H(1)···Si(1) interaction for Δ-[*cis*-Ru((*R*,*R*)-Me-DuPHOS)$_2$(Et$_2$SiH)(H)] and Δ-[*cis*-Ru((*R*,*R*)-Me-DuPHOS)$_2$(PhSiH$_2$)(H)] but not for their Ru(*R*,*R*-BPE)$_2$ analogues. Molecular structures were also determined for Λ-[*cis*-Ru((*R*,*R*)-Me-BPE)$_2$(Bpin)(H)], Λ-[Ru((*S*,*S*)-Me-DuPHOS)$_2$(η^2-C$_2$H$_4$)], Δ-[Ru((*R*,*R*)-Me-DuPHOS)$_2$(η^2-C$_2$H$_4$)], and *trans*-[Ru((*R*,*R*)-Me-DuPHOS)$_2$(C$_6$F$_5$)(H)]. In situ laser photolysis in the presence of *p*-H$_2$ generates hyperpolarized NMR spectra because of magnetically inequivalent hydrides; these experiments and low temperature photolysis with D$_2$ reveal that the loss of hydride ligands is concerted. The reaction intermediates [Ru(DuPHOS)$_2$] and [Ru(BPE)$_2$] were detected by laser flash photolysis and have spectra consistent with approximate square-planar Ru(0) structures. The rates of their reactions with H$_2$, D$_2$, HBpin, and PhSiH$_3$ were measured by transient kinetics. Rate constants are significantly faster for [Ru(BPE)$_2$] than for [Ru(DuPHOS)$_2$] and follow the substrate order H$_2$ > D$_2$ > PhSiH$_3$ > HBpin.

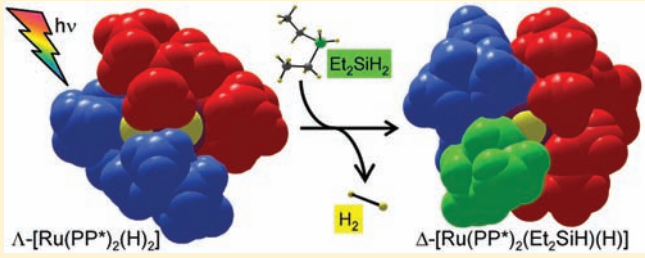

INTRODUCTION

Many studies of chemistry at metals with bidentate ligands leave the configuration (Λ or Δ) at the metal uncontrolled, with the consequence that there may be two or more isomers present throughout the study. A recent survey of asymmetric coordination chemistry for octahedral complexes presents synthetic methods of controlling the stereochemistry at the metal.[1] Synthetic and helicity control of optically pure complexes is achieved through use of well designed bridging or chiral ligands.[2] Among the many studies addressing the systematic control of stereochemistry at the metal, those of von Zelewsky were notable for their link to the photophysics.[3,4] A recent study of chiral nitrogen ligands on Ru(II), Zn(II), and Fe(II) includes circularly polarized absorption and emission and time-dependent density functional theory.[5] While most of the structural studies concern complexes with nitrogen ligands, Halpern et al. demonstrated the applicability to complexes of the type Ru(PP*)(carboxylate)$_4$ (PP* = *R*-BINAP).[6] Extensive studies by Brunner of optically active half-sandwich metal complexes include structural studies, circular dichroism, mechanisms of epimerization, and asymmetric catalysis.[7] Asymmetric synthesis is the dominant application of chiral ligands, especially with phosphorus donor atoms,[8] but typical synthetic methodology aims to create vacant sites at the metal, leaving the configuration at the metal unknown. We recently used dynamic NMR spectroscopy on a chiral monodentate phosphine to reveal the epimerization at the metal in half sandwich rhodium complexes generated by photoinduced B−H and H−H activation.[9] We showed by means of DFT calculations that the epimerization occurred by η^2-B−H or η^2-H−H structures in the transition states. Pregosin and Albinati have used chiral bidentate phosphines in association with NMR spectroscopy to study mechanistic issues, especially ion-pairing.[10] In this study, we report the effect of chiral bidentate phosphines on the photoinduced oxidative addition at complexes of the type [Ru(PP*)$_2$H$_2$] (PP* = (*R*,*R*)-Me-BPE, (*R*,*R*)-Me-DuPHOS, and (*S*,*S*)-Me-DuPHOS, Scheme 1). The use of chiral ligands allows us to probe the stereochemistry much more thoroughly than with achiral ligands both in solution (circular dichroism) and in the crystalline state. We find that the configuration at the metal is determined by

Received: November 10, 2011
Published: January 24, 2012

   dx.doi.org/10.1021/ja210568t | *J. Am. Chem. Soc.* 2012, 134, 3480−3497

Scheme 1. Ligand Structures (a) (*R*,*R*)-Me-BPE, (b) (*R*,*R*)-Me-DuPHOS, and (c) (*S*,*S*)-Me-DuPHOS

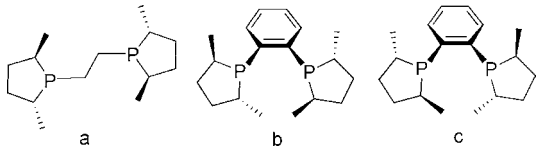

the ligand configuration and that the kinetics of reaction are strongly influenced by the steric demands of the ligand.

The steady state and laser flash photochemistry of *cis*- or *trans*-$[Ru(PP)_2(H)_2]$ (PP = $R_2PCH_2CH_2PR_2$, R = CH_3 (dmpe), C_2H_5 (depe), C_6H_5 (dppe), C_2F_5 (dfepe)) type complexes has been studied intensively in our group.[11] By employing inert matrices and laser flash experiments, we have demonstrated the loss of H_2 and formation of a transient $[Ru(PP)_2]$ with a square planar configuration at Ru upon irradiation with broad band UV light. The intermediates $[Ru(PP)_2]$ are exceptionally well suited to transient absorption investigation, since they exhibit a rich optical absorption spectrum with several bands spanning the visible region. The reaction rates measured in the presence of substrates (H_2, CO, Et_3SiH, C_2H_4, HBpin (pin = pinacolate)) are influenced by the nature of the substituent on the phosphorus atom and by the substrate, resulting in an increase in reactivity in the following order: $Ru(dfepe)_2$ < $Ru(dppe)_2$ < $Ru(depe)_2$ < $Ru(dmpe)_2$. Steady-state solution photochemistry revealed that the transient reacts with substrates to give addition or oxidative addition products, but none of the products resulted from activation of solvent (C_6D_6, THF, heptane).[11a,d,e] We have also reported the effect of a C_1 bridge in place of a C_2 bridge[12] and shown that competing photodissociation of phosphine is favored in solution over the dissociation of the dihydride ligand for *cis*-$[Ru(PMe_3)_4(H)_2]$.[11f] The same methodology has also been applied to $Fe(dmpe)_2H_2$ and $Os(dmpe)_2H_2$.[11g,h]

Laser flash photolysis was also employed on dihydride complexes of tetradentate phosphines $[M(PP_3)(H)_2]$ (M = Ru, Os; PP_3 = $P(CH_2CH_2PPh_2)_3$). Notably, $[Ru(PP_3)]$ undergoes cyclometalation in the absence of substrate and oxidative addition with benzene, whereas $[Os(PP_3)]$ does not undergo cyclometalation but forms oxidative addition products with alkanes and with benzene.[11i]

Related ruthenium carbonyl dihydride complex $[Ru(PPh_3)_3(CO)(H)_2]$ and $[Ru(etp)(CO)(H)_2]$ (etp = $PhP(CH_2CH_2PPh_2)_2$) studied by laser flash photolysis revealed reductive elimination of the hydride ligands,[13a,b] but when a carbene is incorporated $[Ru(PPh_3)_2(IEt_2Me_2)(CO)(H)_2]$ (IEt_2Me_2 = 1,3-bis(ethyl)-4,5-dimethylimidazol-2-ylidene), the photochemistry is different. Further mechanistic information has been obtained by employing para-hydrogen induced polarization (PHIP) of NMR spectra.[13c] Competing loss of ligands also occurs in Ru(0) complexes such as $[Ru(dppe)(PPh_3)(CO)_2]$.[13c]

For $[Ru(PPh_3)_3(CO)(H)_2]$ and $[Ru(PH_3)_4(H)_2]$ complexes, DFT studies of photodissociation of H_2 showed fast (100 fs) elimination when the system is constrained to freeze the Ru−H and H−H distances.[14] In another report, DFT calculations showed that the calculated UV/vis spectra of $[Ru(PH_3)_4]$ reproduce the experimental ones with a square planar geometry around ruthenium. The reactivity of $[Ru(PH_3)_4]$ was modeled for addition of H_2 and CO and found to be very exothermic in both cases, with an η^1 approach for H_2 to the $[Ru(PH_3)_4]$ at an early stage of the reaction which changes to η^2 at later stages.[14]

There are just two reports of ruthenium $[Ru(PP^*)_2]$ (PP* = (*R*,*R*)-Me-BPE, (*R*,*R*)-Me-DuPHOS, (*S*,*S*)-Me-DuPHOS) hydride complexes with BPE ligands: one is *trans*-$[Ru((R,R)\text{-Me-BPE})_2(PMePh)(H)]$, while the other one is the coordinatively unsaturated cationic $[Ru((R,R)\text{-Me-BPE})_2(H)][(BPh_4)]$; both of them are used in catalytic asymmetric alkylation reaction of secondary phosphines with good enantioselectivity.[15] The complexes were characterized by NMR spectroscopy, but their crystal structures were not determined. For the DuPHOS analogues, the literature is not rich either. The neutral *cis*-$[Ru((R,R)\text{-Me-DuPHOS})_2(H)_2]$ Λ-*R*,*R*-Ru2H$_2$ complex was characterized by NMR spectroscopy together with cationic complexes *trans*-$[Ru((R,R)\text{-Me-DuPHOS})_2(\eta^2\text{-}H_2)(H)]PF_6$ and *trans*-$[Ru((R,R)\text{-Me-DuPHOS})_2(N_2)(H)]PF_6$, which were studied by X-ray crystallography.[16] Another chiral neutral dihydride complex bearing a diphosphinite ligand, *rac*-$[Ru(Ph_2POC_6H_{10}OPPh_2)_2(H)_2]$, has been reported along with its crystal structure.[17]

In this study, we aimed to follow up our mechanistic studies of rhodium complexes with chiral monodentate phosphines with an investigation of photoinduced oxidative addition at ruthenium complexes with chiral bidentate phosphines. We chose BPE and DuPHOS[18] because they contain no functionalities other than alkyl and aryl groups, and they contain the same phospholane ring, {PhP(2*R*,5*R*-$Me_2C_4H_6$)}, as that used in our previous studies at Rh.[9] We have synthesized the dihydride complexes Λ-[*cis*-Ru((*R*,*R*)-Me-BPE)$_2$(H)$_2$], Λ-*R*,*R*-Ru1H$_2$, Δ-[*cis*-Ru((*S*,*S*)-Me-DuPHOS)$_2$(H)$_2$], Δ-*S*,*S*-Ru2H$_2$, and Λ-[*cis*-Ru((*R*,*R*)-Me-DuPHOS)$_2$(H)$_2$], Λ-*R*,*R*-Ru2H$_2$, and studied their photoinduced reactions. The reactions include examples of B−H, Si−H, and C−H bond activation to $[Ru(PP^*)_2]$, as well as addition of CO and C_2H_4. All complexes reported here are *cis* complexes unless otherwise stated. When compared to earlier studies of *cis*-$[Ru(PP)_2H_2]$, we have introduced new probes of stereochemistry (circular dichroism and crystallographic determination of configuration) and new probes of mechanism (PHIP and competition reactions), in addition to conventional NMR studies and laser flash photolysis used previously. We show that the ligands control the configuration at the metal and exercise steric control over substrate attack.

RESULTS

Starting Materials. Complexes Λ-[*cis*-Ru((*R*,*R*)-Me-BPE)$_2$(H)$_2$] Λ-*R*,*R*-Ru1H$_2$, Δ-[*cis*-Ru((*S*,*S*)-Me-DuPHOS)$_2$(H)$_2$], Δ-*S*,*S*-Ru2H$_2$, and Λ-[*cis*-Ru((*R*,*R*)-Me-DuPHOS)$_2$(H)$_2$] Λ-*R*,*R*-Ru2H$_2$ were synthesized by Grubbs' method by heating $[Ru(COD)Cl_2]_x$, the corresponding chiral bidentate phosphine, and NaOH in 2-butanol at 80 °C overnight.[19] Isolation and purification afforded Λ-*R*,*R*-Ru1H$_2$ as an off-white powder; Δ-*S*,*S*-Ru2H$_2$ and Λ-*R*,*R*-Ru2H$_2$ are isolated as yellow crystalline materials. Since Δ-*S*,*S*-Ru2H$_2$ and Λ-*R*,*R*-Ru2H$_2$ are enantiomers, their NMR data are identical. Selected NMR data are summarized in Table 1, and full data are given in the Experimental Section.

In both cases, the NMR spectra show that the reaction generates a single *cis* dihydride product. The proton NMR spectrum of Λ-*R*,*R*-Ru1H$_2$ exhibits two distinct quartets and two overlapping doublets of doublets resonances for pairs of equivalent methyl groups of the chelating phospholane ligand. Their patterns result from coupling to phosphorus (J_{PH} = 12−16 Hz) and to protons ($J_{HH} \approx 7$ Hz). In $^1H\{^{31}P\}$ spectra, each of these resonances appears as a doublet. The quartets probably arise from virtual coupling to mutually *trans* P nuclei and approximately equal coupling to an

dx.doi.org/10.1021/ja210568t | J. Am. Chem. Soc. 2012, 134, 3480−3497

Table 1. NMR Spectrocopic Data [Solvent C_6D_6, δ (J/Hz)] for Dihydrides

	Λ-*R*,*R*-Ru1H$_2$	Δ-*S*,*S*-Ru2H$_2$ Λ-*R*,*R*-Ru2H$_2$
^{1}H hydride	−10.7 m	−10.0 m
^{31}P{^{1}H}	101.5 t, J_{PP} 17	103.3 t, J_{PP} 20
	96.8 t, J_{PP} 17	100.1 t, J_{PP} 20

adjacent proton. The hydride region shows a second-order multiplet pattern at δ −10.7 consistent with C_2 symmetry. The coupling constants were extracted with the help of the experimental values for *cis*-J_{PP}, selective ^{31}P decoupling, and simulation with *g*NMR (Figure 1, upper).[20] With an estimated value of *trans*-J_{PP} = 200 Hz, we

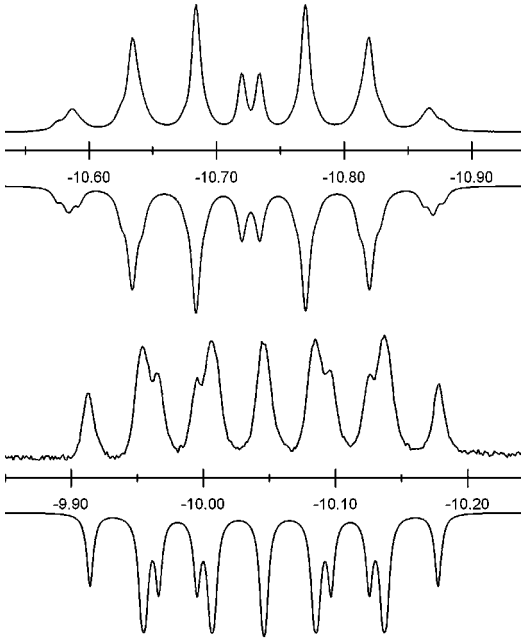

Figure 1. Hydride region of 500 MHz ^{1}H NMR with simulated spectrum (down) and experimental spectrum (up) in C_6D_6 at 300 K: top, Λ-*R*,*R*-Ru1H$_2$; bottom, Λ-*R*,*R*-Ru1(Et$_2$SiH)(H). Full coupling constants are presented in the Experimental Section.

matched the experimental spectrum in the hydride region with *cis*-$^2J_{PH}$ = 25 Hz and *trans*-$^2J_{PH}$ = 68 Hz (see the Experimental Section). Complete decoupling from phosphorus reveals a singlet consistent with two equivalent *cis* protons. The ^{31}P{^{1}H} NMR spectrum shows two sets of triplet resonances for two pairs of equivalent phosphorus atoms with J_{PP} of 17 Hz.

The only report of a neutral ruthenium dihydride bearing a chiral phospholane concerned the deprotonation of *trans*-[Ru(*R*,*R*)-Me-DuPHOS)$_2$(η^2-H$_2$)(H)]PF$_6$ with *n*-BuLi to give Λ-*R*,*R*-Ru2H$_2$.[16] The present results for Δ-*S*,*S*-Ru2H$_2$ and Λ-*R*,*R*-Ru2H$_2$ are consistent with the literature and will not be discussed further, but full data are given in the Experimental Section.

We synthesized both enantiomers of the DuPHOS complexes in order to elucidate the configuration at the metal center for starting materials and photoproducts. The absorption and CD spectra of Λ-*R*,*R*-Ru1H$_2$ only show features at very short wavelengths (see Supporting Information, Figure S1), but the spectra of Δ-*S*,*S*-Ru2H$_2$ and Λ-*R*,*R*-Ru2H$_2$ are more informative. The absorption spectra for Δ-*S*,*S*-Ru2H$_2$ and Λ-*R*,*R*-Ru2H$_2$ in hexane have a maximum at 323 nm ($\varepsilon = 4.6 \times 10^3$ dm^3 mol^{-1} cm^{-1}) with a tail to longer wavelength. The CD spectrum for the *R*,*R* isomer displays five features: 379 nm ($\Delta\varepsilon$ = −0.3 dm^3 mol^{-1} cm^{-1}), 336 nm ($\Delta\varepsilon$ = −1.1), 292 nm ($\Delta\varepsilon$ = −0.9), 279 nm ($\Delta\varepsilon$ = 1.5), and 251 nm ($\Delta\varepsilon$ = −10.7). The *S*,*S* analogue has the same CD spectra but of opposite sign, as expected (Figure 2, top). A full table of CD results is given in the Supporting Information.

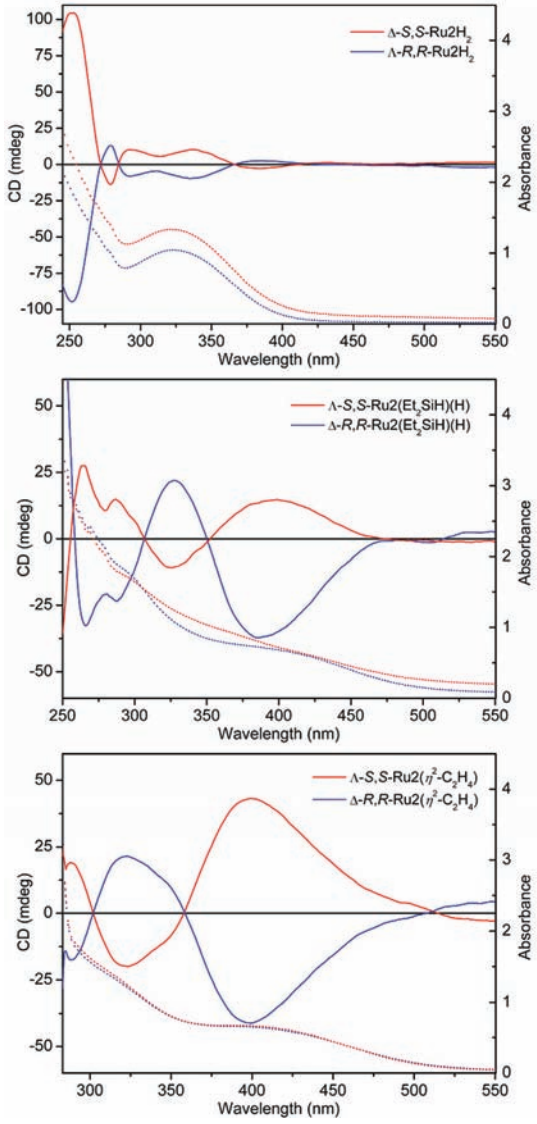

Figure 2. CD (full lines) and UV (dotted lines) spectra: top, Δ-*S*,*S*-Ru2H$_2$ (red) and Λ-*R*,*R*-Ru2H$_2$ (blue); middle, Λ-*S*,*S*-Ru2(Et$_2$SiH)(H) (red) and Δ-*R*,*R*-Ru2(Et$_2$SiH)(H) (blue) all in hexane; bottom, Λ-*S*,*S*-Ru2(η^2-C$_2$H$_4$) (red) and Δ-*R*,*R*-Ru2(η^2-C$_2$H$_4$) (blue) in toluene.

Although several X-ray structures are known for ruthenium coordinated to just one DuPHOS ligand,[10,21] there are only two structures containing two ligands per ruthenium center, *trans*-[Ru(*R*,*R*)-Me-(DuPHOS)$_2$(η^2-H$_2$)(H)]PF$_6$ and *trans*-[Ru-(*R*,*R*)-Me-(DuPHOS)$_2$(N$_2$)(H)]PF$_6$, and none for BPE.[16] The X-ray structures of Λ-*R*,*R*-Ru1H$_2$, Δ-*S*,*S*-Ru2H$_2$, and Λ-*R*,*R*-Ru2H$_2$ are described in a dedicated section together with those of the photoproducts.

Steady State Photolysis. To our surprise, photolysis in the presence of Et$_3$SiH did not result in any products. On using a smaller substrate, Et$_2$SiH$_2$, the reaction proceeds with formation of hydride products as expected. This selective reactivity can be associated with the steric bulk of the bidentate phosphine

dx.doi.org/10.1021/ja210568t | J. Am. Chem. Soc. 2012, 134, 3480−3497

ligands, which blocks access to the metal center. Thus, photochemical reaction of Λ-*R*,*R*-Ru1H_2, Δ-*S*,*S*-Ru2H_2, and Λ-*R*,*R*-Ru2H_2 complexes is possible only with careful choice of the substrates. There is no thermal reaction at room temperature between these ruthenium dihydrides and any of the substrates discussed below other than C_6F_5Br.

With this in mind, we carried out detailed studies of the irradiation of the dihydride complexes in the presence of two small silanes Et_2SiH_2 and $PhSiH_3$ (Scheme 2). Irradiation of

Scheme 2. Photochemical Reactions of Λ-*R*,*R*-Ru1H_2, Δ-*S*,*S*-Ru2H_2, and Λ-*R*,*R*-Ru2H_2

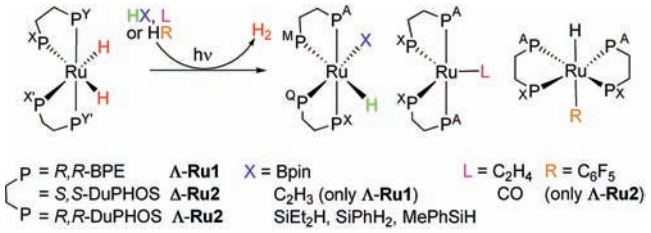

Λ-*R*,*R*-Ru1H_2 in C_6D_6 solution and Et_2SiH_2 at room temperature resulted in the appearance of a new hydride signal in the ^{1}H NMR spectrum at δ −10.0 as a multiplet due to the coupling to four inequivalent phosphorus atoms (Figure 1, lower). On decoupling from phosphorus, the spectrum shows a singlet for the hydride ligand assigned to the Λ-*R*,*R*-Ru1(Et_2SiH)(H) product. The proton attached to silicon atom shows a broad resonance at δ 3.9, but the ^{1}H{^{31}P} NMR spectrum reveals a broad triplet ($J_{HH} \approx 4$ Hz).

The ^{31}P{^{1}H} NMR spectrum supports the formation of a *cis* product, displaying four resonances in an AXMQ pattern. The resonances of the mutually *trans* phosphorus atoms (P_A and P_X) are coupled to one another and further split by the other ^{31}P nuclei (δ_A 104.9 doublet of pseudotriplets J = 224, 25 Hz, δ_X 82.1 doublet of pseudotriplets J = 224, 21 Hz). The remaining two resonances (δ 90.5 and 88.0) appear as pseudoquartets due to the approximate equal coupling to three inequivalent phosphorus atoms.

A ^{1}H−^{29}Si HMQC NMR correlation, with no proton decoupling, linked the Si*H* at δ 3.9 peak to a ^{29}Si resonance at δ 23.4 which is shifted downfield compared to the free silane (δ −22.9). The coupling constant J_{SiH} for the silyl hydride (140 Hz) is reduced relative to that of the free silane (184 Hz). The silicon−phosphorus splitting is observed as a passive coupling (J_{PSi} 139 Hz) in the silicon dimension with ^{1}H decoupling. The value of J_{SiH} for the hydride was determined as 8 Hz by ^{1}H−^{29}Si{^{31}P} correlation.

Photolysis of Λ-*R*,*R*-Ru2H_2 in the presence of diethylsilane proceeds in a similar manner; NMR data suggest as major product the silyl hydride, Δ-*R*,*R*-Ru2(Et_2SiH)(H). The reaction of Δ-*S*,*S*-Ru2H_2 with Et_2SiH_2 revealed the formation of the silyl hydride product with the same NMR data. The CD spectra of the two enantiomers (Figure 2, middle) show that the first two Cotton effect bands at 385 nm (−37.2 mdeg) at 328 nm (+22.0 mdeg) for Δ-*R*,*R*-Ru2(Et_2SiH)(H) are more intense and have opposite signs compared to the CD of starting dihydrides, which suggests a change in configuration at ruthenium.

The photoreaction in C_6D_6 in the presence of phenyl silane occurs with clean conversion to the silyl hydride Λ-*R*,*R*-Ru1($PhSiH_2$)(H), suggested by similar characteristic NMR data. The metal hydride signal has an almost identical pattern to that from the diethylsilane reaction, and the diastereotopic hydrogens bonded to silicon are well separated, with one appearing as a pseudodoublet of quartets at δ 4.8 and the other one as a multiplet at δ 4.5 (coupling to one another and to ^{31}P). They correlate in the ^{1}H−^{29}Si HMQC spectrum with a ^{29}Si resonance at δ −18.1 with J_{SiH} 146 Hz and J_{PSi} 163 Hz.[22] The value of J_{SiH} for the metal hydride was determined as 8 Hz by ^{1}H−^{29}Si{^{31}P} correlation. The pattern of the hydride signal for Δ-*R*,*R*-Ru2($PhSiH_2$)(H) is almost identical to that observed for Δ-*R*,*R*-Ru2(Et_2SiH)(H). The hydrogens bonded to the silicon atom are less separated, with each one appearing as multiplets. The ^{1}H−^{29}Si HMQC NMR spectrum of Δ-*R*,*R*-Ru2($PhSiH_2$)(H) correlated the SiH_2 protons to a ^{29}Si resonance at δ −23.9 (compare free silane at δ −60) and shows coupling constants J_{SiH} = 147 Hz (free silane J_{SiH} 200 Hz) and J_{PSi} = 159 Hz (Figure 3). The

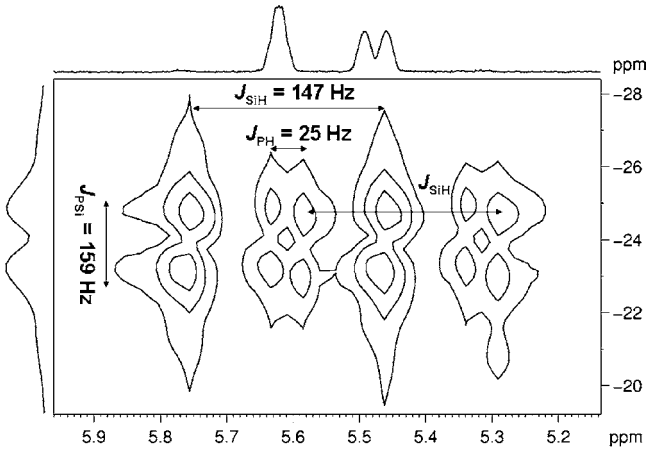

Figure 3. 2D ^{1}H−^{29}Si HMQC spectrum showing the alkyl region of Δ-*R*,*R*-Ru2($PhSiH_2$)(H) in C_6D_6 at 300 K with the ^{1}H spectrum shown on the *x*-axis. Note that the 1D ^{1}H spectrum projected onto the *x*-axis shows the resonances of the ^{28}Si isotopomer whereas the 2D spectrum shows the resonances of the ^{29}Si isotopomer.

^{31}P NMR spectrum of Δ-*R*,*R*-Ru2($PhSiH_2$)(H) is similar to that of Λ-*R*,*R*-Ru1($PhSiH_2$)(H) except that the resonances for the mutually *trans* phosphorus nuclei lie much closer to one another and exhibit features of an AB quartet with each component split into apparent triplets. The crystal structure was determined for each of the silyl hydride products (see crystallographic section).

When Λ-*R*,*R*-Ru1H_2 is photolyzed in the presence of a prochiral silane, $MePhSiH_2$, the proton NMR spectrum shows formation of two hydrides as multiplets, two resonances for the *ortho*-phenyl protons, and two distinct resonances for the SiH protons, all of which are simplified by ^{31}P decoupling. The ^{31}P{^{1}H} NMR spectra display two sets of four resonances in an AXMQ pattern. All of these pairs of resonances are present in a ratio of ca. 2:1. They are assigned to Λ-*R*,*R*-Ru1($MePhSi^RH$)(H) and Λ-*R*,*R*-Ru1($MePhSi^SH$)(H), where Si^R and Si^S represent the chirality at silicon (we cannot identify the dominant isomer). Analogous experiments carried out with Λ-*R*,*R*-Ru2H_2 yielded similar results, but the resonances for the two isomers were closer together in the ^{1}H spectra and the ratio of isomers was ca. 1:1.

Another substrate which is small enough to react with these complexes is C_2H_4. The ^{31}P{^{1}H} NMR spectrum recorded after photolysis (30 min) of Λ-*R*,*R*-Ru1H_2 in C_6D_6 with 1 atm of ethene shows two sets of triplets at δ 96.6 and 84.4 (J_{PP} = 26 Hz)

dx.doi.org/10.1021/ja210568t | J. Am. Chem. Soc. 2012, 134, 3480−3497

as major product resonances assigned to the ethene complex, Λ-*R*,*R*-Ru1(η^2-C_2H_4), together with two further triplets δ 89.3 and 80.3 (J_{PP} = 28 Hz) belonging to the vinyl hydride complex *trans*-*R*,*R*-Ru1(C_2H_3)(H) and traces of *cis* vinyl hydride. The vinyl hydride complexes are stable at room temperature under an ethene atmosphere. On prolonged photolysis, the only product formed is Λ-*R*,*R*-Ru1(η^2-C_2H_4). The ^{1}H NMR spectrum shows formation of ethane (C_2H_6) and *trans*-*R*,*R*-Ru1(C_2H_3)(H) as the conspicuous products together with traces of *cis*-*R*,*R*-Ru1(C_2H_3)(H) and starting material. The protons of the coordinated ethene in Λ-*R*,*R*-Ru1(η^2-C_2H_4) overlap with those of the BPE ligand. In the hydride region, a quintet δ −12.2 (J_{PH} = 22 Hz) signals the *trans* vinyl hydride isomer. The resonances corresponding to the vinyl group appear as complex multiplets. However, in the ^{1}H{^{31}P} NMR spectrum, they are simplified and appear at δ 5.6 (RuCH$_a$CH$_b$*H*$_c$, J_{HaHc} = 20 Hz, J_{HcHb} = 6 Hz), 6.7 (RuCH$_a$-C*H*$_b$H$_c$, J_{HaHb} = 13 Hz, J_{HbHc} = 6 Hz), and 8.3 (RuC*H*$_a$CH$_b$H$_c$, J_{HaHc} = 20 Hz, J_{HaHb} = 13 Hz), indicating a vinyl group similar to that of reported achiral analogues.[11a−c,23]

In contrast, photolysis of a C_6D_6 solution of Λ-*R*,*R*-Ru2H$_2$ in the presence of an ethene atmosphere forms exclusively the η^2-C_2H_4 complex Δ-*R*,*R*-Ru2(η^2-C_2H_4). The ^{31}P{^{1}H} NMR spectrum displays a A_2X_2 spin system with two sets of triplet resonances at δ 95.0 and 69.8 (J_{PP} = 30 Hz). When the solvent used for photolysis was changed to hexane, orange crystals precipitated and were analyzed by X-ray crystallography (see below). The same experiments were performed for Δ-*S*,*S*-Ru2H$_2$ but only the CD spectra would differentiate between the isomeric [Ru(η^2-C_2H_4)] products (Figure 2, bottom). The first two Cotton effect bands for the *R*,*R* isomer at 399 nm ($\Delta\varepsilon$ = −3.7 dm^3 mol^{-1} cm^{-1}) and 323 nm ($\Delta\varepsilon$ = 1.9) are broad, are very intense, and have opposite sign to the starting materials.

In similar experiments, the photochemical reactions of the ruthenium dihydrides were studied in the presence of CO. The BPE analogue generated the pentacoordinate Ru(0)(CO) complex together with some byproduct and release of some free diphosphine. The ^{31}P{^{1}H} NMR spectrum for the Λ-*R*,*R*-Ru1(CO) at room temperature shows two broad resonances which sharpen at 280 K into two sets of triplets δ 104.5 and 88.0 with J_{PP} = 31 Hz. The DuPHOS dihydrides Λ-*R*,*R*-Ru2H$_2$ and Δ-*S*,*S*-Ru2H$_2$ react with CO cleanly to form bright red complexes Λ-*R*,*R*-Ru2(CO) and Δ-*S*,*S*-Ru2(CO) characterized by two sharp phosphorus resonances (δ 92.0 and 78.6 t, J_{PP} = 35 Hz) at room temperature. Thus, Λ-*R*,*R*-Ru2(CO) and Δ-*S*,*S*-Ru2(CO) are rigid while Λ-*R*,*R*-Ru1(CO) is fluxional. The UV spectra of Λ-*R*,*R*-Ru2(CO) and Δ-*S*,*S*-Ru2(CO) have broad maxima at 475 nm, and the signs of the CD bands between 300 and 400 nm are opposite to those of the ethene products (see the Supporting Information).

Interest in catalytic borylation of alkanes and arenes persuaded us to use HBpin as substrate.[24] Photolysis conducted in NMR tubes in hexane or C_6D_6 at room temperature in the presence of either Λ-*R*,*R*-Ru1H$_2$ or Λ-*R*,*R*-Ru2H$_2$ produces new hydrides assigned to oxidative addition products, Λ-*R*,*R*-Ru1(Bpin)(H) and Λ-*R*,*R*-Ru2(Bpin)(H) supported by the following spectroscopic data. In both cases, the hydride region of the ^{1}H NMR spectra shows a multiplet which simplifies to a singlet on decoupling from phosphorus. The ^{31}P{^{1}H} NMR spectra (Figure S6 of the Supporting Information) display four resonances characteristic of an AXMQ pattern, with the signal for phosphorus *trans* to boron atom being broad. The mutually *trans* phosphorus atoms appear as doublets of triplets split with J_{PP} 237 and 16 Hz, and the signal for the phosphorus *trans* to hydride ligand is an apparent quartet with J_{PP} 16 and 18 Hz (values for Λ-*R*,*R*-Ru1H$_2$). The ^{11}B NMR spectrum reveals a broad signal around δ 50 characteristic of a metal boryl complex.[25] A ^{1}H−^{13}C HMQC correlation of Λ-*R*,*R*-Ru1(Bpin)-(H) shows that the methyl resonance at δ 1.1 correlates to the quaternary carbon δ 79.3 within the Bpin moiety. The spectroscopic evidence is similar to that for the *cis* boryl hydrides, [Ru(depe)$_2$(Bpin)(H)] and [Ru(dmpe)$_2$(Bpin)(H)], previously reported.[11d] The conclusions are confirmed by the crystal structure of Λ-*R*,*R*-Ru1(Bpin)(H).

We also intended to study an aromatic C−H bond activation reaction. In order to maximize the bond strength of the Ru−C bond of the product,[26] we selected pentafluorobenzene as a substrate, but only Λ-*R*,*R*-Ru2H$_2$ reacted with it photochemically in C_6D_6 solution and the NMR data indicate formation of *trans*-*R*,*R*-Ru2(C_6F_5)(H). The hydride region of the ^{1}H spectrum shows a broad multiplet at δ −13.1 without a large *trans* J_{PH} coupling, which simplifies to a triplet with J_{HF} of 13 Hz on decoupling from ^{31}P. The ^{31}P{^{1}H} NMR spectrum shows two very close resonances (δ 86.0 and 84.4 m) because the two pairs of mutually *trans* phosphorus nuclei are not equivalent to one another. They appear as multiplets with a small coupling to each other and to fluorine. The resonances corresponding to the coordinated C_6F_5 group in the ^{19}F NMR spectrum are well separated, δ −85.4, −164.5, −165.5, and show an upfield shift compared to the free ligand. The crystal structure was also determined.

The photoreactions of Λ-*R*,*R*-Ru1H$_2$ and Λ-*R*,*R*-Ru2H$_2$ with CH_2Cl_2 and with C_6F_5Br provided evidence for formation of *trans*-*R*,*R*-Ru1(Cl)(H), *cis*-*R*,*R*-Ru2(Cl)(H), *trans*-*R*,*R*-Ru2-(Cl)(H), *cis*-*R*,*R*-Ru1(Br)(H), *trans*-*R*,*R*-Ru1(Br)(H), *cis*-*R*,*R*-Ru2(Br)(H), and *trans*-*R*,*R*-Ru2(Br)(H). The results are presented in the Supporting Information.

Solid-State Structures. Single crystals of Λ-*R*,*R*-Ru1H$_2$, Δ-*S*,*S*-Ru2H$_2$, Λ-*R*,*R*-Ru2H$_2$, Λ-*R*,*R*-Ru1(Et_2SiH)(H), Δ-*R*,*R*-Ru2(Et_2SiH)(H), Λ-*R*,*R*-Ru1($PhSiH_2$)(H), Δ-*R*,*R*-Ru2($PhSiH_2$)-(H), Λ-*R*,*R*-Ru1(Bpin)(H), Δ-*R*,*R*-Ru2(η^2-C_2H_4), Λ-*S*,*S*-Ru2(η^2-C_2H_4), *trans*-*R*,*R*-Ru2(C_6F_5)(H), *trans*-*R*,*R*-Ru1(Br)(H), and *trans*-*R*,*R*-Ru1(Cl)$_2$ were grown by slow evaporation of hexane solutions (dichloromethane solution for *trans*-*R*,*R*-Ru1(Cl)$_2$) and were analyzed by X-ray diffraction.

The numbering scheme of the phosphorus atoms for all the structures follows the following rules: P(2)P(3) are mutually *trans*, P(1) *trans* to heavy atom, and P(4) *trans* to hydride. The two chelate rings are specified as P(1)P(2) and P(3)P(4). All the structures of hydrides display an octahedral (or distorted octahedral) geometry around the stereogenic ruthenium center, and the hydrides were located for all the structures by difference maps. The molecular structures of the dihydrides Λ-*R*,*R*-Ru1H$_2$, Δ-*S*,*S*-Ru2H$_2$, and Λ-*R*,*R*-Ru2H$_2$ (Figure 4 and Supporting Information) showed that the complexes adopt a distorted octahedral geometry around ruthenium, with the hydride ligands occupying *cis* positions and the methyl groups of the phospholane rings bending toward them. The distortion of the structures from an ideal octahedron is a steric effect associated with the bulk of the phospholane ligand. To a reasonable approximation, the overall structure retains the C_2 symmetry element of the metal center and ligands.

The structure of Λ-*R*,*R*-Ru1H$_2$ is complicated by disorder of the phospholane ring containing P(3) and the carbon atoms bonded to it. They were modeled over two positions in a 50:50 ratio, restrained to be approximately isotropic, and constrained to have the same ADP; the Ru−P(3) and Ru−P(3b) distances

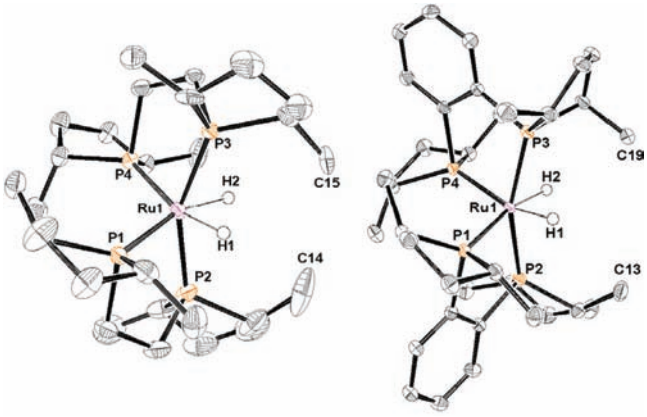

Figure 4. Molecular structures of Λ-*R*,*R*-Ru1H_2 (left) and Λ-*R*,*R*-Ru2H_2 (right) (50% thermal ellipsoids), all hydrogen atoms omitted for clarity except for H(1) and H(2). Note that one phosphine ring in Λ-*R*,*R*-Ru1H_2 is disordered (see text); one form is shown.

were restrained to be equal. The mutually *trans* Ru−P bonds are far from collinear, with an angle P(2)−Ru(1)−P(3) of 154.33(4)°, and the *cis* angle between phosphorus atoms on different ligands P(1)−Ru-P(4) is 111.40(2)° (Table 2). These angles are smaller than those for the dppe (161.5, 106.9°)[27] and the phosphinite analogues (158.3, 97.17°).[17] The structure of Λ-*R*,*R*-Ru2H_2 reveals that the hydride ligands are less sterically hindered than those for Λ-*R*,*R*-Ru1H_2 due to the rigid benzene backbone. The geometry around ruthenium is closer to octahedral than that for Λ-*R*,*R*-Ru1H_2 with P(2)−Ru(1)−P(3) 160.74(4)° and P(1)−Ru−P(4) 104.28(2)°. The benzene rings are arranged opposite to each other with a 79° angle between their planes. The tendency for the methyl groups to embrace the hydride ligands may be measured by the angle C(13)···Ru(1)···C(19) of 68.75(6)°. The corresponding angle for Λ-*R*,*R*-Ru1H_2 C(14)···Ru(1)···C(15) is smaller at 55.69(9)°. These angles highlight the steric hindrance controlling the access to the metal center for large substrates (see photolysis section), although the rigidity of the skeletons also needs to be taken into account (see Supporting Information for the molecular structure of Δ-*S*,*S*-Ru2H_2 and space filling models).

The molecular structure of Λ-*R*,*R*-Ru1(Et_2SiH)(H) shows that the Λ configuration around ruthenium is retained (Figure 5) and the surrounding geometry is closer to octahedral than that of the starting material (Table 2). The hydride crystallized with two independent molecules in the asymmetric unit. In one of them, the carbon atoms of the phospholane ring containing P(1) are disordered; they have been modeled over two positions in an 84:16 ratio. The Ru(1)−Si(1) bond length of 2.4496(7) Å is in agreement with that found in [Ru(PMe_3)$_4$(SiR_3)(H)].[28] The distance between the silicon atom and the hydride ligand of 2.74(3) Å indicates that there is no residual interaction.[29] The hydrogen atom bonded to silicon (Si(1)−H(1a) = 1.53(3) Å) points away from the metal center. For Δ-*R*,*R*-Ru2(Et_2SiH)(H) there are some differences. The absolute configuration is Δ, opposite to that of starting material Λ-*R*,*R*-Ru2(H)$_2$, and the angles around ruthenium are very different: P(1)−Ru(1)−Si(1) and P(4)−Ru(1)−Si(1) are 159.55(2)° and 89.69(2)° in Λ-*R*,*R*-Ru1(Et_2SiH)(H) but 144.31(5)° and 116.08(4)° in Δ-*R*,*R*-Ru2(Et_2SiH)(H), respectively. Associated with this change, is a reduction in the hydride−silicon distance H(1)···Si(1) to 2.04(5) Å for Δ-*R*,*R*-Ru2(Et_2SiH)(H), indicating a residual interaction.

The molecular structures of Λ-*R*,*R*-Ru1($PhSiH_2$)(H) and Δ-*R*,*R*-Ru2($PhSiH_2$)(H) (Figure 5, Table 2) resemble those of the silyl hydride analogues discussed above. The configuration is retained for Λ-*R*,*R*-Ru1($PhSiH_2$)(H) but not for Δ-*R*,*R*-Ru2($PhSiH_2$)(H). Again, the rigid benzene backbone makes the access of phenyl silane to the ruthenium center difficult, resulting in less complete oxidative cleavage of the Si−H bond. This feature is reflected in the angles P(1)−Ru(1)−Si(1) (146.61(2)°) and P(4)−Ru(1)−Si(1) (111.57(2)°) and the H(1)···Si(1) separation of 2.20(4) Å compared to those in Λ-*R*,*R*-Ru1($PhSiH_2$)(H) of 164.14(3)°, 87.12(2)°, and 2.79(3) Å, respectively.

The molecular structure of Λ-*R*,*R*-Ru1(Bpin)(H) (Figure 5) shows that the geometry around ruthenium is a distorted octahedron and the configuration is retained as Λ. The hydride ligand was located at 1.56(2) Å from Ru(1) (Table 3). A search

Table 2. Selected Bond Lengths (Å) and Angles (deg) for Λ-*R*,*R*-Ru1H_2, Δ-*S*,*S*-Ru2H_2, Λ-*R*,*R*-Ru2H_2, and Their Photoproducts with Silanes

bonds/angles	Λ-*R*,*R*-Ru1H_2	Δ-*S*,*S*-Ru1H_2	Λ-*R*,*R*-Ru2H_2	Λ-*R*,*R*-Ru1(Et_2SiH)(H)	Λ-*R*,*R*-Ru1($PhSiH_2$)(H)	Δ-*R*,*R*-Ru2(Et_2SiH)(H)	Δ-*R*,*R*-Ru2($PhSiH_2$)(H)
Ru−P(1)	2.3201(6)	2.3050(12)	2.2997(6)	2.3600(6)	2.3447(6)	2.3378(12)	2.3285(5)
Ru−P(2)	2.2817(6)	2.2698(11)	2.2685(7)	2.3383(6)	2.3077(6)	2.3157(11)	2.3103(6)
Ru−P(3)	2.2612(12)	2.2703(11)	2.2697(7)	2.3014(6)	2.2999(6)	2.3082(11)	2.3043(5)
Ru−P(3b)[a]	2.2934(12)						
Ru−P(4)	2.3135(6)	2.3201(14)	2.3138(7)	2.3420(6)	2.3511(6)	2.3634(11)	2.3604(5)
Ru−H(1)	1.47(4)	1.53(5)	1.53(4)	1.47(3)	1.63(3)	1.50 (5)	1.52(3)
Ru−H(2)	1.61(3)	1.63(5)	1.60(4)				
Ru−Si				2.4496(7)	2.4240(7)	2.4608(13)	2.4064(6)
Si···H(1)				2.74(3)	2.79(3)	2.04(5)	2.20(4)
P(1)−Ru−P(2)	85.84(2)	85.87(4)	85.97(2)	83.33(2)	82.76(2)	81.37(4)	81.82(2)
P(1)−Ru−P(3)	108.34(6)	107.52(4)	107.52(2)	96.15(2)	99.63(2)	95.10(4)	96.10(2)
P(1)−Ru−P(4)	111.40(2)	104.44(4)	104.28(2)	110.73(2)	107.36(2)	99.45(4)	101.79(2)
P(2)−Ru−P(3)	154.33(4)	160.74(4)	160.74(2)	172.20(2)	169.92(2)	173.63(4)	174.46(2)
P(1)−Ru−Si				159.55(2)	164.14(3)	144.32(5)	146.61(2)
P(4)−Ru−Si				89.69(2)	87.12(2)	116.08(4)	111.57(2)
P(1)−Ru−H(2)	163.1(10)	170.9(16)	167.5(12)				
P(4)−Ru−H(1)	163.6(13)	161(3)	162.7(16)	171.1(11)	168.0(10)	171.2(17)	171.7(9)

[a]See text.

dx.doi.org/10.1021/ja210568t | *J. Am. Chem. Soc.* 2012, 134, 3480−3497

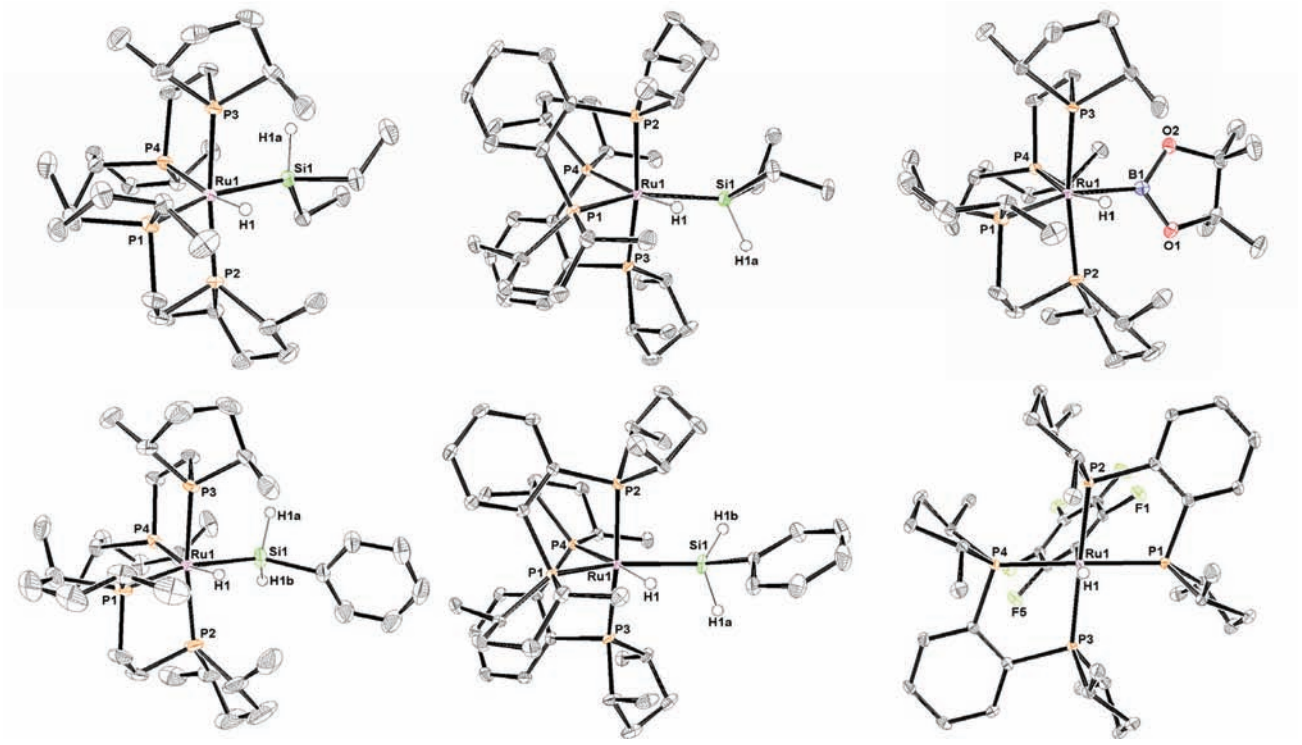

Figure 5. Molecular structures of Λ-*R*,*R*-Ru1(Et_2SiH)(H), top left; Δ-*R*,*R*-Ru2(Et_2SiH)(H), top middle; Λ-*R*,*R*-Ru1(Bpin)(H), top right; Λ-*R*,*R*-Ru1($PhSiH_2$)(H), bottom left; Δ-*R*,*R*-Ru2($PhSiH_2$)(H), bottom middle; *trans*-*R*,*R*-Ru2(C_6F_5)(H), bottom right (50% thermal ellipsoids); all hydrogen atoms omitted for clarity except for H(1), H(1a), and H(1b). One phosphine ring in Λ-*R*,*R*-Ru1(Et_2SiH)(H) is disordered (see text); one form is shown.

Table 3. Selected Bond Lengths (Å) and Angles (deg) for Λ-*R*,*R*-Ru1(Bpin)(H), Λ-*S*,*S*-Ru2(η^2-C_2H_4), Δ-*R*,*R*-Ru2(η^2-C_2H_4), *trans*-*R*,*R*-Ru2(C_6F_5)(H), *trans*-*R*,*R*-Ru1(Br)(H), and *trans*-*R*,*R*-Ru1$(Cl)_2$

bonds/angles	Λ-*R*,*R*-Ru1(Bpin)(H)	Λ-*S*,*S*-Ru2(η^2-C_2H_4)	Δ-*R*,*R*-Ru2(η^2-C_2H_4)	*trans*-*R*,*R*-Ru2(C_6F_5)(H)	*trans*-*R*,*R*-Ru1(Br)(H)	*trans*-*R*,*R*-Ru1$(Cl)_2$
Ru−P(1)	2.3511(5)	2.3107(5)	2.3128(6)	2.3351(6)	2.3383(14)	2.3668(6)
Ru−P(2)	2.3187(4)	2.3166(4)	2.3084(6)	2.3314(6)	2.3108(13)	2.3656(7)
Ru−P(3)	2.2899(4)	2.3084(4)	2.3189(6)	2.3242(6)	2.3181(13)	2.3645(7)
Ru−P(4)	2.3256(4)	2.3126(4)	2.3116(6)	2.3398(6)	2.3192(14)	2.3780(7)
Ru−H(1)	1.56(2)	-	-	1.68(2)	1.47(4)	-
Ru−E	2.117(2)	2.1872(16)	2.195(2)	2.229(2)	2.6675(9)	2.4309(6)
(B/C/Cl/Br)		2.1941(17)	2.188(2)			2.4353(6)
P(1)−Ru−P(2)	83.73(2)	81.157(14)	81.03(2)	83.65(2)	83.17(4)	83.09(2)
P(1)−Ru−P(3)	98.80(1)	95.792(15)	96.28(2)	95.66(2)	97.86(5)	101.40(2)
P(1)−Ru−P(4)	111.95(2)	103.661(15)	103.64(2)	175.96(2)	175.16(5)	175.52(2)
P(2)−Ru−P(3)	170.18(2)	175.396(16)	175.43(2)	161.71(2)	170.66(5)	175.25(2)
P(1)−Ru−E	157.02(6)	145.82(5)	146.42(6)	91.93(6)	88.32(4)	91.17(2)
P(4)−Ru−E	90.40(6)	146.48(5)	145.81(6)	92.11(6)	96.15(4)	94.61(2)
P(4)−Ru−H(1)	163.7(8)			88.6(8)	84.0(17)	

of the CCDC (1st September 2011) revealed no crystal structure with a [$RuP_4B(O_2R)$] fragment, but three for ruthenium boryl (boronate ester) hydrides. They are described as σ-borane-(dihydroborate) for [$Ru(PCy_3)_2((\mu\text{-}H)_2Bpin)(\sigma\text{-}HBpin)(H)$] and σ-boranes for [$Ru(PCy_3)_2(\eta^2\text{-}HBpin)(\eta^2\text{-}H_2)(H)_2$] and [$Ru(PCy_3)_2(\eta^2\text{-}HBcat)(\eta^2\text{-}H_2)(H)_2$].[30] The crystallographic data for Λ-*R*,*R*-Ru1(Bpin)(H) provide a Ru−B bond distance of 2.117(2) Å (compare sum of the covalent radii of Ru and B: 2.13 Å), that is similar to that in the σ-borane complexes. The angle between the [O,O] centroid, B, and Ru (174.4°) lies between the corresponding angles of the σ-borane (171.5°) and that of the dihydridoborate (177.1°). The B(1)···H(1) separation of 2.29(2) Å and the Ru−H distance indicates a classical boryl hydride, unlike the σ-boranes, which have B−H distances of 1.2−1.3 Å. The angle between the two planes, one defined by [OOBRu] and the other by Ru−P(1)−P(4), is 70.27°.

For Δ-*R*,*R*-Ru2(η^2-C_2H_4), the ethene is bonded almost symmetrically in the equatorial site of a trigonal bipyramid (Figure S13 of the Supporting Information, Table 3) with Ru−C bond lengths of 2.188(2) Å and 2.195(2) Å. The angle between the two planes, one defined by metallacyclopropane ring Ru−C(37)−C(38) and the other by Ru−P(1)−P(4), is 15.84°. The Ru−P bond lengths are almost equal, ranging from 2.3084(6) to 2.3189(6) Å, while the ethene bond C(37)−C(38) is 1.423(3) Å, comparable to that in [$Ru(PMe_3)_4(C_2H_4)$].[31] The molecular

dx.doi.org/10.1021/ja210568t | *J. Am. Chem. Soc.* 2012, 134, 3480−3497

structure of Λ-*S*,*S*-Ru2(η^2-C_2H_4) is given in the Supporting Information (Figure S13).

There are only two crystal structures in CCDC containing the fragment [$RuP_2(C_6F_5)H$]: one of them being the achiral analogue *trans*-[$Ru(dmpe)_2(C_6F_5)(H)$],[32] while the other one is a *cis* carbene complex [$Ru(dppp)(ICy)(CO)(C_6F_5)(H)$][33] (ICy = 1,3-dicyclohexylimidazol-2-ylidene). The molecular structure of *trans*-*R*,*R*-Ru2(C_6F_5)(H) is shown in Figure 5 (and the space filling model is shown in the Supporting Information). The Ru−C bond length (2.229(2) Å) lies in between those reported for the other structures. The C_6F_5 plane almost bisects the C−C bonds of the C_6H_4 units of the DuPHOS ligands. The angle between the plane defined by the C_6F_5 group and the Ru−H bond vector is 6.39°. The RuP_4 skeleton is significantly distorted from planarity, with a torsional angle of 18.4° between the planes Ru−P(1)−P(2) and Ru−P(3)−P(4). The hydride was located at 1.68(2) Å from Ru, compared to a Ru−H distance of 1.59(5) Å found in the dmpe complex.

The molecular structures of *trans*-*R*,*R*-Ru1(Br)(H) and *trans*-*R*,*R*-Ru1$(Cl)_2$ are reported in the Supporting Information.

MECHANISTIC STUDIES

Competition Reactions. Competition experiments were used to determine the kinetic selectivity for different oxidative addition reactions. They were run in NMR tubes in C_6D_6 in the presence of 10 equiv of each substrate and followed by NMR spectra measured every 30 min. The product ratios were determined from the integrals of the hydride resonances in the $^1H\{^{31}P\}$ spectra. Λ-*R*,*R*-Ru1H_2 and Λ-*R*,*R*-Ru2H_2 were photolyzed in the presence of either HBpin and Et_2SiH_2 or HBpin and $PhSiH_3$. For the reactions with Et_2SiH_2 and HBpin, the results show that both complexes have a preference of 4 to 1 for activation of the B−H bond. When using HBpin and the smaller silane $PhSiH_3$, the selectivity changed dramatically in favor of Si−H bond cleavage in a 9 to 1 ratio for both complexes. This indicates an order of kinetic selection of $PhSiH_3$ > HBpin > Et_2SiH_2. To check that one silane reacts faster than the other, another experiment was performed with both silanes. The selectivity for the smaller substrate is confirmed: both complexes show reaction with $PhSiH_3$ but virtually no reaction with Et_2SiH_2. Control experiments were run with a sample of Λ-*R*,*R*-Ru1(Et_2SiH)(H) in the presence of either HBpin or $PhSiH_3$ and a sample of Δ-*R*,*R*-Ru2($PhSiH_2$)(H) in the presence of HBpin or Et_2SiH_2 in C_6D_6 solutions. No thermal reaction was observed after 48 h, but photochemical exchange did occur (30 min photolysis), clearly demonstrated by the reduction of one hydride resonance and growth of the other. The formation of free diethylsilane or phenylsilane could also be observed. For the latter example, a trace of Λ-*R*,*R*-Ru2H_2 formation was observed. The product distribution in the control experiments is consistent with that in the competition experiments.

Photochemical Reactions of Λ-*R*,*R*-Ru2H_2 with D_2 and *p*-H_2. In order to elucidate if the H_2 elimination mechanism is concerted, we have studied the photochemical reactivity of Λ-*R*,*R*-Ru2H_2, under a D_2 atmosphere and under *p*-H_2.

Deuterium gas (5 bar) was added to a dilute cyclopentane solution of Λ-*R*,*R*-Ru2H_2 in an NMR tube. No exchange was observed in the absence of photolysis. Cyclopentane was chosen because it freezes at a very low temperature and has a singlet proton resonance that is well suited to solvent suppression. The sample was irradiated in situ at 355 nm with a Nd:YAG laser at low temperature.[34] The reaction was followed by ^2H NMR and by ^1H NMR spectroscopy; the ^1H NMR spectra were recorded with solvent suppression at 600 MHz. The ^1H NMR spectrum before photolysis showed the hydride multiplet at δ −10.0, a trace of HD detected by its signal at δ 4.7 with J_{HD} 42 Hz, and a trace of H_2 (δ 4.8 s) (present as impurities in the D_2). The initial ^2H NMR spectrum exhibited a resonance for D_2 at δ 4.7 and a resonance at δ 1.6 for deuterated solvent present in natural abundance. After photolysis (7 min) at 180 K, the ^1H NMR signal for H_2 grows considerably, while the signal for HD is unchanged (standardized on aromatic protons). The hydride resonance is reduced in intensity slightly (from 2.0 to 1.86), and the ^2H NMR spectrum shows a small signal at δ −10.0 in the deuteride region. The sample was warmed to 210 K and irradiated for a further 7 min. The trends observed previously were continued: growth of H_2 (from 0.1 to 0.18), depletion of the hydride resonance (from 1.86 to 1.82), and growth of the deuteride resonance. The deuteride signal appears as a broad singlet, as expected considering that the largest coupling $J_{PDtrans}$ is ca. 11 Hz. In addition, the signal of D_2 decreases relative to the ^2H signal of the solvent. There is no change in the amount of HD. These measurements are consistent with concerted elimination of H_2 and oxidative addition of D_2 to form Λ-*R*,*R*-Ru2D_2 (eq 1).

$$[Ru(DuPHOS)_2]H_2 + D_2 \xrightarrow{h\nu} [Ru(DuPHOS)_2]D_2 + H_2 \quad \text{(eq 1)}$$

Another similar experiment was conducted with photolysis at 273 K. After 5 min of irradiation, the ^1H NMR spectrum showed marked growth in the signals of H_2 and of HD and a decrease in the hydride resonance. The ^2H NMR spectrum shows growth of the deuteride resonance. The sample was warmed to 295 K, and the spectra were recorded. The ^1H NMR spectrum showed HD and a trace of the hydride resonance but no H_2. The ^2H NMR spectrum showed D_2, the deuteride resonance, and HD at δ 4.4 with a coupling constant J_{HD} of 42.8 Hz. In contrast to the low temperature experiments, the photolysis of the sample at 273 K displays H/D scrambling in the ^1H NMR spectrum (see Discussion section).

In addition to the experiments with D_2, *p*-H_2 assisted ^1H NMR studies were carried out. A solution of Λ-*R*,*R*-Ru2H_2 in benzene-d_6 was placed in an NMR tube. The resulting solution was degassed, and the tube was filled with *p*-H_2 (3 bar). After irradiation of the sample for 10 s in situ at 355 nm at 295 K, the ^1H NMR spectrum displays a PHIP-enhanced hydride resonance at δ −10.0 for the hydride and for free H_2 at δ 4.4 (Figure 6). An OPSY experiment[35] was measured afterward under the same conditions, but after 30 s of photolysis. In this type of experiment, only the resonance of H_2 and the enhanced resonances are observed. The OPSY spectrum exhibits just two resonances, one for H_2 at δ 4.4 and another one at −10.0 corresponding to hydrides (Figure 6). The magnetization was transferred to phosphorus, allowing us to record a $^{31}P\{^1H\}$ NMR spectrum with PHIP-enhancement.[36] This spectrum exhibited a prominent phosphorus resonance at δ 100.1 that is assigned to the phosphorus *trans* to hydride and a weaker resonance for the remaining phosphorus nuclei (see the Supporting Information). There is slight enhancement of the resonance of the phosphorus *cis* to hydride at δ 103.0. The PHIP enhancement observed in these experiments provides direct evidence that photochemical elimination and readdition of H_2 is concerted (see Discussion).

Laser Flash Photolysis. The transient photochemistry of Λ-*R*,*R*-Ru1H_2 and Λ-*R*,*R*-Ru2H_2 was investigated on nanosecond

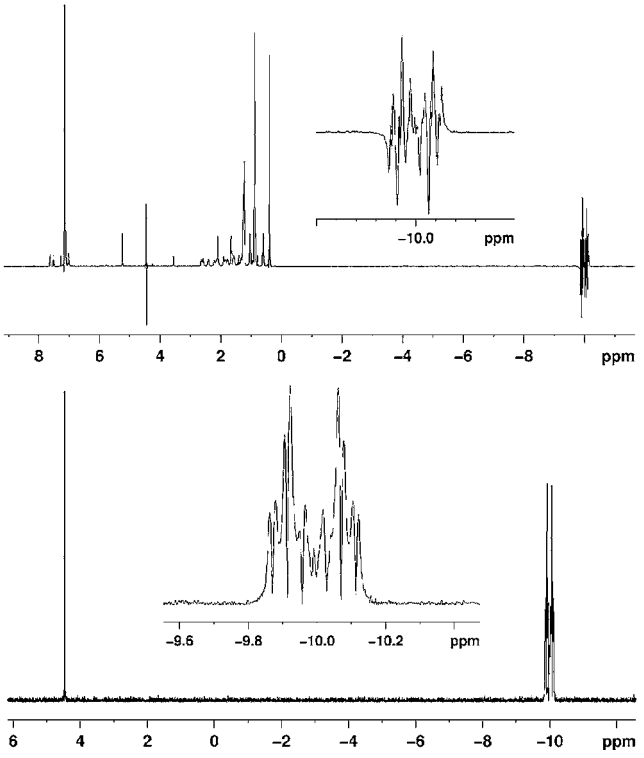

Figure 6. Above: ^{1}H NMR spectrum of Λ-*R*,*R*-Ru2H$_2$ in C_6D_6 obtained at 295 K during photolysis under a *p*-H_2 atmosphere. Below: OPSY experiment recorded under the same conditions (details of the hydride resonances are shown in the inset).

and microsecond time scales in order to determine the UV/vis spectra of the reaction intermediates of the type $[Ru(PP)_2]$ and to determine the rates of reaction of the intermediates with hydrogen and with the substrates used in the steady state reactions. Reactions were initiated with a XeCl laser (308 nm, 10 ns pulse width), and spectra were recorded point-by-point in cyclohexane solution at 295 K.

The spectra of the transient species formed from Λ-*R*,*R*-Ru1H$_2$ and Λ-*R*,*R*-Ru2H$_2$ were recorded under a hydrogen atmosphere (1 atm) in order to ensure the complete reversibility of the reaction. The transient spectra derived from both the dihydride complexes exhibit at least three absorption maxima between 400 and 800 nm and resemble those recorded previously for other complexes of the type $[Ru(PP)_2]$.[11] The decay kinetics of the transients were measured at each of the maxima, confirming that they were indistinguishable and that they rose within the instrument response time. They are assigned to a single intermediate in each case, $[Ru(BPE)_2]$ and $[Ru(DuPHOS)_2]$, respectively. The most intense lies at 500 nm for $[Ru(BPE)_2]$ and 560 nm for $[Ru(DuPHOS)_2]$; there is a long wavelength feature at 740 nm for $[Ru(BPE)_2]$ and at 700 nm for $[Ru(DuPHOS)_2]$ (Figure 7a, b).

Laser flash photolysis of Λ-*R*,*R*-Ru1H$_2$ and Λ-*R*,*R*-Ru2H$_2$ under argon results in the formation of the transient species, which decay with pseudo-first-order kinetics over a time scale of hundreds of microseconds (1.1×10^4 s^{-1}) for Λ-*R*,*R*-Ru1H$_2$ or even milliseconds (2.6×10^3 s^{-1}) for Λ-*R*,*R*-Ru2H$_2$. However, after laser flash photolysis of Λ-*R*,*R*-Ru1H$_2$ and Λ-*R*,*R*-Ru2H$_2$ under a hydrogen atmosphere, the transient absorbance returns to the baseline, restoring the initial absorbance, indicating back reaction with H_2. The transients decay with pseudo-first-order kinetics (Figure 7c, d) on a time scale of *ca.* 40 μs (Λ-*R*,*R*-Ru1H$_2$) and *ca.* 100 μs (Λ-*R*,*R*-Ru2H$_2$). Complexes Λ-*R*,*R*-Ru1H$_2$ and Λ-*R*,*R*-Ru2H$_2$ have also been tested under higher pressures of hydrogen (from 1 to 5 bar), and both of the resulting transients

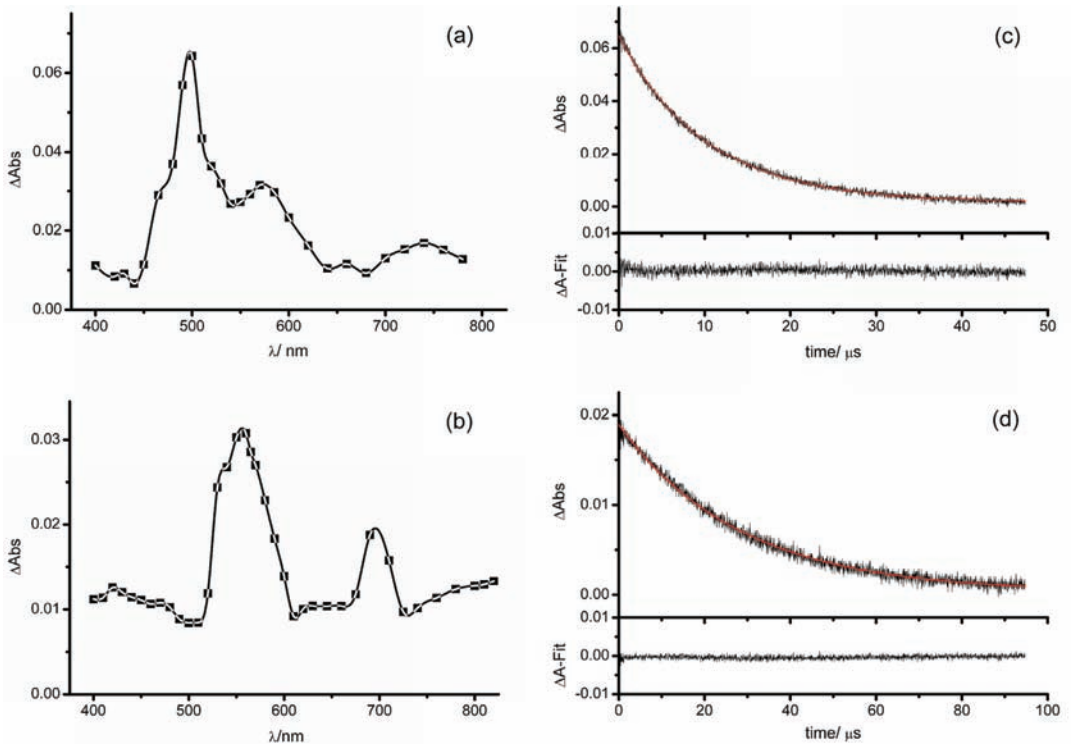

Figure 7. Left: transient UV/vis spectra measured point-by-point at 295 K in cyclohexane on laser flash photolysis under 1 atm H_2 (308 nm) of: (a) Λ-*R*,*R*-Ru1H$_2$ and (b) Λ-*R*,*R*-Ru2H$_2$. Right: transient decay after photolysis of (c) Λ-*R*,*R*-Ru1H$_2$ recorded at 500 nm and (d) Λ-*R*,*R*-Ru2H$_2$ followed at 560 nm. The red lines show the fit to first-order kinetics. The differences between the observed and the fitted decays are shown under the transient decays.

dx.doi.org/10.1021/ja210568t | *J. Am. Chem. Soc.* 2012, 134, 3480−3497

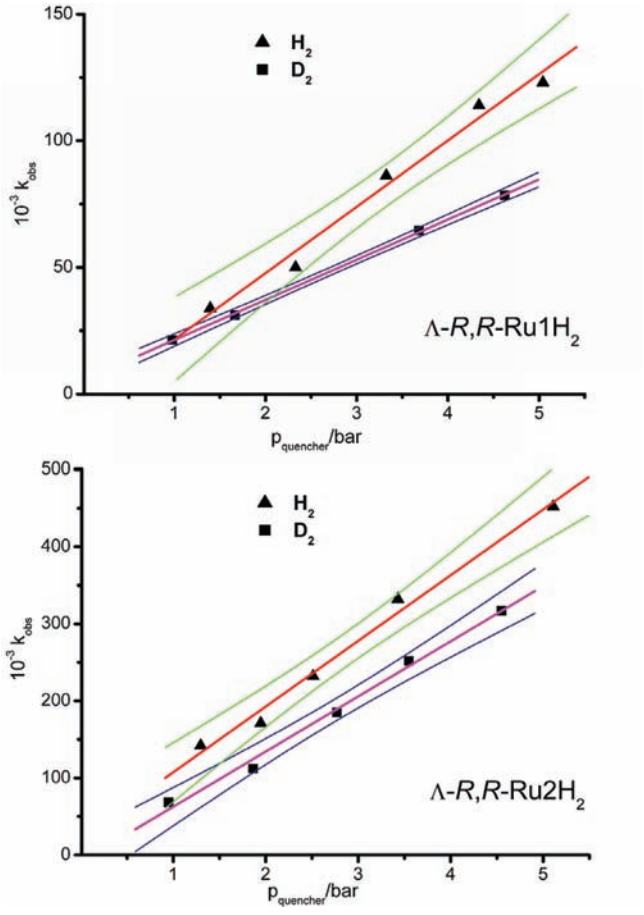

Figure 8. Plots of pseudo-first-order rate constants for the decay of the transients obtained upon laser flash photolysis (308 nm) of complexes Λ-*R*,*R*-Ru1H$_2$ and Λ-*R*,*R*-Ru2H$_2$ in cyclohexane vs the pressure of quenching gas (H$_2$ and D$_2$). The lines through the points show the best fits, and the colored lines show the 95% confidence limits.

showed a linear dependence plot of k_{obs} versus $p(H_2)$ (Figure 8). The second-order rate constants, k_2, for the regeneration of the precursor in the presence of hydrogen were determined to be $(1.8 \pm 0.1) \times 10^7$ dm^3 mol^{-1} s^{-1} for [Ru(BPE)$_2$] and $(5.6 \pm 0.4) \times 10^6$ dm^3 mol^{-1} s^{-1} for [Ru(DuPHOS)$_2$]. The solubility of H$_2$ was taken as 4.7×10^{-3} mol dm^{-3} atm^{-1}.[37] The kinetic isotopic effects were investigated, under different deuterium pressures (from 1 to 5 bar, Figure 8, Table 4). The KIEs are small for both intermediates

Table 4. Second-Order Rate Constants and Kinetic Isotope Effects for Reactions of Transient Species at 295 K in Cyclohexane

	k_2, dm^3 mol^{-1} s^{-1}	
quencher	Λ-*R*,*R*-Ru1H$_2$	Λ-*R*,*R*-Ru2H$_2$
H$_2$	$(1.8 \pm 0.1) \times 10^7$	$(5.6 \pm 0.4) \times 10^6$
D$_2$	$(1.52 \pm 0.07) \times 10^7$	$(3.37 \pm 0.05) \times 10^6$
k_{H_2}/k_{D_2}	1.2 ± 0.1	1.6 ± 0.1
PhSiH$_3$	$(5.9 \pm 0.4) \times 10^5$	$(1.10 \pm 0.9) \times 10^5$
HBpin	$(9.90 \pm 0.6) \times 10^4$	$(1.05 \pm 0.5) \times 10^4$
C_6F_5H		$(3.06 \pm 0.6) \times 10^3$

but slightly greater for [Ru(DuPHOS)$_2$] (1.6 ± 0.1) than for complex [Ru(BPE)$_2$] (1.2 ± 0.1).[38] The second-order rate constant for reaction of [Ru(DuPHOS)$_2$] with H$_2$ was also determined in benzene as solvent and was found to be insignificantly different from the value measured in cyclohexane. The spectra and reactivity of [Ru(PP*)$_2$] toward hydrogen are consistent with prompt photoelimination of H$_2$ and thermal regeneration of [Ru(PP*)$_2$(H)$_2$] at room temperature under H$_2$ (Scheme 3).

Scheme 3. Photodissociation of H$_2$ and Regeneration of the Starting Material upon Laser Flash Photolysis

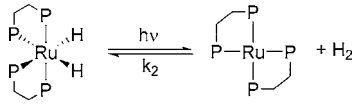

Laser flash photolysis in the presence of HBpin of Λ-*R*,*R*-Ru1H$_2$ and Λ-*R*,*R*-Ru2H$_2$ resulted in rapid quenching of the transient for both Λ-*R*,*R*-Ru1H$_2$ and Λ-*R*,*R*-Ru2H$_2$. The formation and the decay of the transients were followed at the absorption maximum under Ar with a range of borane concentrations (see Supporting Information). The measured absorbance differences always return to the baseline after several microseconds, indicating that the transient complex is completely consumed, leading to Ru(II) product. Plots of k_{obs} against [HBpin] were linear and gave second-order rate constants for Λ-*R*,*R*-Ru1H$_2$ of $(9.90 \pm 0.6) \times 10^4$ dm^3 mol^{-1} s^{-1} and $(1.05 \pm 0.5) \times 10^4$ dm^3 mol^{-1} s^{-1} for Λ-*R*,*R*-Ru2H$_2$. Analogous measurements with PhSiH$_3$ showed that the transient is quenched 10 times faster than in the presence of HBpin (Table 4). A rate constant k_2 of $(3.06 \pm 0.6) \times 10^3$ was determined for the reaction of [Ru(DuPHOS)$_2$] in the presence of pentafluorobenzene. The corresponding measurement was not possible for [Ru(BPE)$_2$], since no reaction occurs.

The effect of ethene (1 atm) on the transient kinetics was investigated for Λ-*R*,*R*-Ru2H$_2$. The transient decayed with pseudo-first-order kinetics back to the baseline. Similar results were obtained with a cyclohexane solution of Λ-*R*,*R*-Ru2H$_2$ under 1 atm of CO. The values are not very different from those obtained under an Ar atmosphere, and the characteristic residual absorbance of Ru(0) complexes was not observed, suggesting that these substrates are poor quenchers for [Ru(DuPHOS)$_2$].

DISCUSSION

Synthesis and Photochemistry. The synthesis and photochemistry of Λ-[*cis*-Ru((*R*,*R*)-Me-BPE)$_2$(H)$_2$] Λ-*R*,*R*-Ru1H$_2$, Δ-[*cis*-Ru((*S*,*S*)-Me-DuPHOS)$_2$(H)$_2$] Δ-*S*,*S*-Ru2H$_2$, and Λ-[*cis*-Ru((*R*,*R*)-Me-DuPHOS)$_2$(H)$_2$] Λ-*R*,*R*-Ru2H$_2$ follow the pattern established for other complexes of the type [Ru(PP)$_2$(H)$_2$],[11] but they are more selective with respect to substrate, and the reactions yield a single ruthenium epimer. The photochemical reactions are summarized in Schemes 2 and 4. In this study, we have used circular

Scheme 4. Configuration at the Ru Center upon Photolysis

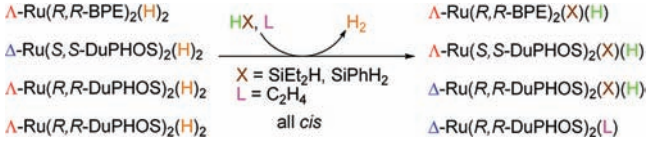

dichroism, competition studies, and *p*-H$_2$ induced polarization (PHIP) in addition to the NMR and laser flash methods used in our previous studies, and we have obtained far more extensive crystallographic characterization.

dx.doi.org/10.1021/ja210568t | J. Am. Chem. Soc. 2012, 134, 3480−3497

Stereochemistry in Solution and Crystalline State. In all our experiments, we employed chiral phosphines. The ruthenium atom in these bis chelate complexes provides a further stereogenic center in addition to the two stereogenic carbon atoms on each diphosphine. The NMR spectra of Λ-*R*,*R*-Ru1H_2, Δ-*S*,*S*-Ru2H_2, and Λ-*R*,*R*-Ru2H_2 each show a single hydride resonance attributed to a C_2 symmetric *cis*-dihydride as the exclusive species. The $^{31}P\{^1H\}$ NMR spectra also point to a single stereoisomer of the dihydrides. The DuPHOS complexes Δ-*S*,*S*-Ru2H_2 and Λ-*R*,*R*-Ru2H_2 show identical NMR spectra but opposite circular dichroism, as expected for mirror image complexes. The CD spectra are far richer than the UV absorption spectra, with five CD maxima but only one clear absorption maximum between 250 and 400 nm for Δ-*S*,*S*-Ru2H_2 and Λ-*R*,*R*-Ru2H_2. The assignment of these spectra is beyond the scope of this paper, but our measurements establish that the transitions involve the metal centers, since the CD spectra are quite distinct from those of the free ligands *R*,*R*-DuPHOS and *S*,*S*-DuPHOS (the *S*,*S* ligand shows broad bands with a positive Cotton effect with maxima at 320 and 245 nm and one negative Cotton effect at 263 nm—see the Supporting Information).[39] Thus, the solution spectra point to the dominance of a single isomer with high optical purity at metal and ligand (no other isomer within limits of NMR detection). The crystal structures of the dihydride complexes identify the configurations at ruthenium.

The complexes react photochemically with a primary silane ($PhSiH_3$), a secondary silane (Et_2SiH_2), and a borane (HBpin) to give *cis* oxidative addition products. The crystal structures indicate that the methyl groups of the phosphine ligands prevent reactions with tertiary silanes by steric hindrance. Each of the products is formed as a single isomer, as is evident from the CD and NMR spectra. Intriguingly, the BPE silyl hydride complexes retain the configuration of their dihydride precursors, whereas the DuPHOS silyl hydride complexes show the opposite configuration at ruthenium (Scheme 4). Since the reactions proceed via square planar [Ru(PP*)$_2$], the mechanism provides an opportunity for such a change of configuration (see below). The crystal structures of the DuPHOS complexes show P—Ru—Si angles further from the ideal octahedral angles and much closer contacts between silicon and the hydride than the BPE complexes, consistent with residual Si···H interactions for the DuPHOS complexes.

The photochemical reactions using the prochiral silane ($MePhSiH_2$) show formation of two diastereoisomers at Si with a 2:1 ratio for BPE but 1:1 for DuPHOS. Elution of Λ-*R*,*R*-Ru1(SiMePhH)(H) through an alumina column with toluene and hexane as eluents gives different ratios of the products, indicating some separation (ratio is always measured in C_6D_6). The overall ratio of the isomers is preserved. These observations indicate that there is no exchange between isomers.

The BPE boryl hydride again retains the configuration at Ru. While we have not succeeded in crystallizing the DuPHOS boryl hydride, the CD spectra suggest that this complex retains the configuration at Ru (see the Supporting Information). Unlike the boryl hydride complexes of rhodium with a chiral monodentate phosphine,[9] there is no evidence for any dynamic rearrangement at the metal.

We have succeeded with two C—H activation reactions: Λ-*R*,*R*-Ru1H_2 reacts with ethene to form *cis* and *trans* isomers of the vinyl hydride *R*,*R*-Ru1(C_2H_3)(H). The reaction of Λ-*R*,*R*-Ru2H_2 with pentafluorobenzene yields *trans*-*R*,*R*-Ru2(C_6F_5)(H). Although it is reasonable to surmise that *cis*-*R*,*R*-Ru2(C_6F_5)(H) is formed initially, we have not observed it. The reasons for the complete absence of *R*,*R*-Ru2(C_2H_3)(H) and *R*,*R*-Ru1(C_6F_5)(H) are not known.

The photoreaction of Λ-*R*,*R*-Ru2H_2 with ethene yields Δ-*R*,*R*-Ru2(η^2-C_2H_4) exclusively. As is typical for Ru(0) complexes, this complex is red, with a prominent long wavelength absorption. Notably, the corresponding CD spectra show a very conspicuous broad band at the same wavelength. This band may be assigned to a metal-to-ligand charge-transfer transition. The signs of the CD transitions above 350 nm are opposite to those of the starting dihydrides and the same as those of the silyl hydride analogues.

The reactions with CO yield the expected Ru(0) carbonyls. The ^{31}P NMR spectra of Λ-*R*,*R*-Ru1(CO) show evidence for axial—equatorial exchange at room temperature through line broadening, whereas those of Λ-*R*,*R*-Ru2(CO) show no evidence for exchange. This observation provides direct evidence that the DuPHOS complex is more rigid than its BPE counterpart because of the phenylene ring. The low energy MLCT band of Λ-*R*,*R*-Ru2(CO) revealed by circular dichroism lies to even longer wavelength than that of Δ-*R*,*R*-Ru2(η^2-C_2H_4). The sign of the Cotton effect suggests that the Λ configuration is not changed compared to that of the starting dihydride.

Photochemical Mechanism. Three independent lines of evidence indicate that the primary photochemical step is reductive elimination of dihydrogen: (a) the observation of the characteristic multiband UV/vis spectra[11] of the 4-coordinate [Ru(PP*)$_2$] within the instrumental rise time (<20 ns) on laser flash photolysis of Λ-*R*,*R*-Ru1H_2, and Λ-*R*,*R*-Ru2H_2; (b) the formation of hyperpolarized NMR spectra on photolysis of Λ-*R*,*R*-Ru2H_2 under *p*-H_2; (c) the formation of [Ru(DuPHOS)$_2$(D)$_2$] + H_2 but without HD, on photolysis of Λ-*R*,*R*-Ru2H_2 under a D_2 atmosphere at low temperature. We now consider each of these approaches in turn.

Laser Flash Photolysis. Similar multiband spectra for [Ru(PP)$_2$] have been observed previously for PP = dmpe, depe, dppe, and dfepe and have been shown to be characteristic of an approximate square planar geometry. The lowest energy band was previously assigned to a d_{z^2}—p_z transition;[11] it is observed at 740 and 700 nm for Λ-*R*,*R*-Ru1H_2 and Λ-*R*,*R*-Ru2H_2, respectively, close to observations on the analogues. At higher energy, we note that the most intense absorption band of Λ-*R*,*R*-Ru2H_2 is red-shifted significantly (560 nm) relative to the spectra of the other complexes. The crystal structures of the *trans* complexes provide models for the structures of [Ru(BPE)$_2$] and [Ru(DuPHOS)$_2$]. In *trans*-*R*,*R*-Ru1(Cl_2) and *trans*-*R*,*R*-Ru1(Br)(H), the [Ru(BPE)$_2$] moiety approximates to D_2 symmetry (see Supporting Information) while the [Ru(DuPHOS)$_2$] moiety of *trans*-*R*,*R*-Ru2(C_6F_5)(H) shows a significant twisting of Ru—P(1)—P(2) relative to Ru—P(3)—P(4) (18.4°). This torsion, which maintains D_2 symmetry, may account for the shift observed in the UV/vis spectrum.

p-Hydrogen Induced Polarization (PHIP). Observation of PHIP requires overpopulation of the ($\alpha\beta$—$\beta\alpha$) nuclear spin state. Such polarization has been demonstrated for numerous examples of loss of H_2, but the current experiments have some special features. The two hydrides in most examples are chemically inequivalent, but here they are chemically equivalent and PHIP is possible thanks to their magnetic inequivalence.[40] Our PHIP spectra are recorded following in situ laser photolysis under 3 atm *p*-H_2 at 355 nm, as demonstrated previously.[34] The polarization of the hydride proton resonance has also been transferred to phosphorus.[36] Since the polarization is generated entirely within the strong magnetic field, it can be ascribed to the PASADENA

effect.[41] We have also observed some polarization in the resonance of free hydrogen, as has been reported previously when H_2 adds reversibly to a metal.[42] These experiments provide a rigorous demonstration of concerted reductive elimination and readdition of hydrogen.[43] Notice that the PHIP experiments are much more sensitive than the D_2 exchange experiments and require shorter photolysis times.

Exchange with D_2. In situ laser photolysis of Λ-*R*,*R*-Ru2H_2 in the presence of D_2 at very low temperature (180 K) provides straightforward evidence supporting exchange of [Ru(DuPHOS)$_2$(H)$_2$] with D_2 and release of H_2 with negligible formation of HD. The equivalent reaction at 273 K, on the other hand, shows substantial formation of HD, indicating that an additional exchange process is occurring. Since no ^{2}H resonances were observed for exchange into the phosphine, we suggest that the phosphine chelate ring opens reversibly under these conditions, and dihydrogen coordinates to form [Ru(κ^1-DuPHOS)(DuPHOS)(H)$_2$(η^2-D$_2$)]. Such (dihydrogen)-dihydride complexes typically undergo rapid exchange between dihydrogen and hydride ligands;[44] chelate ring closing will then expel HD. This is the only evidence that we have obtained indicating a process competing with photochemical reductive elimination from the dihydride complexes.

Kinetics. The reactivity of the intermediates [Ru(BPE)$_2$] and [Ru(DuPHOS)$_2$] has been explored by transient kinetics. The second-order rate constant for back reaction of [Ru(BPE)$_2$] with H_2 ($(1.8 \pm 0.1) \times 10^7$ dm^3 mol^{-1} s^{-1}) is similar to that for [Ru(dppe)$_2$] but substantially smaller than those for [Ru(dmpe)$_2$] and [Ru(depe)$_2$]. The rate constant for reaction of [Ru(DuPHOS)$_2$] with H_2 is three times smaller than that for reaction with [Ru(BPE)$_2$]. The kinetic isotope effects (KIEs) for these reactions are 1.18 ± 0.08 and 1.63 ± 0.12, respectively. These reactions have very small barriers that are almost certainly created by steric hindrance, and the KIE is correspondingly small.

The rate constants for reaction of the three oxidative addition substrates with [Ru(BPE)$_2$] span a factor of 200 and follow the order H_2 > $PhSiH_3$ > HBpin. The corresponding rate constants for reaction of [Ru(DuPHOS)$_2$] are between three and nine times smaller, but they follow the same order (Figure 9, Table 4).

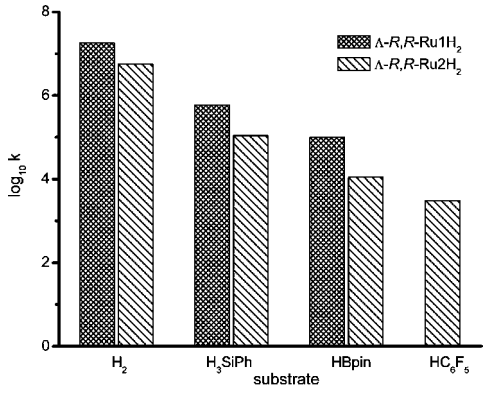

Figure 9. Plot of $\log_{10} k_2$ versus the different quenchers for Λ-*R*,*R*-Ru1H_2 (stipple) and Λ-*R*,*R*-Ru2H_2 (hatched), where k_2 is the second-order rate constant.

Notably, this order still applies if a statistical correction is applied for the number of hydrogen atoms available for activation. The rate constant for reaction of [Ru(DuPHOS)$_2$] with C_6F_5H was even smaller than that for other substrates (1800 times smaller than that for reaction with H_2). The reaction rate with Et_2SiH_2 was too slow to determine by these methods.

The reason that the reactions of [Ru(BPE)$_2$] and [Ru(DuPHOS)$_2$] are slower than those of [Ru(dmpe)$_2$] and [Ru(depe)$_2$] almost certainly lies with the blocking action of the methyl substituents on the phospholane rings (see Figure 4 and the Supporting Information). The evidence of the crystal structures of Λ-*R*,*R*-Ru1H_2 and Λ-*R*,*R*-Ru2H_2 indicates that the steric constraints are greater for Λ-*R*,*R*-Ru1H_2, but it is [Ru(DuPHOS)$_2$] that reacts more slowly, probably because the C_6H_4 link is more rigid than the CH_2CH_2 link between the phosphorus atoms.

In addition to transient kinetic measurements, we performed competition reactions in which we followed the photoreaction of Λ-*R*,*R*-Ru1H_2 or Λ-*R*,*R*-Ru2H_2 in the presence of two substrates. These tests demonstrated that the selectivity $PhSiH_3$ > HBpin > Et_2SiH_2 can be observed in steady state photochemical experiments, just as in transient spectroscopy. However, exchange between substrates also occurs on photolysis of Λ-*R*,*R*-Ru1(Et_2SiH)(H) in the presence of HBpin or $PhSiH_3$, indicating that the product distribution represents a photostationary state.

Mechanism of Epimerization at Ruthenium. The observation of a Λ structure for Λ-*R*,*R*-Ru2H_2 but a Δ structure for Δ-*R*,*R*-Ru2(E)(H) (E = Et_2SiH, $PhSiH_2$) shows that *R*,*R*-DuPHOS can bind to the ruthenium center in either configuration. Moreover, the formation of Δ-[*cis*-*R*,*R*-Ru2(E)(H)] rather than the *trans* isomer indicates that these are kinetic not thermodynamic products. The mechanism by which [Ru(DuPHOS)$_2$] selects a particular configuration may depend on the twist in its structure.[45]

CONCLUSIONS

We have reported the synthesis and photochemistry of C_2-symmetric Λ-[*cis*-Ru((*R*,*R*)-Me-BPE)$_2$(H)$_2$] Λ-*R*,*R*-Ru1H_2, Δ-[*cis*-Ru((*S*,*S*)-Me-DuPHOS)$_2$(H)$_2$] Δ-*S*,*S*-Ru2H_2, and Λ-[*cis*-Ru((*R*,*R*)-Me-DuPHOS)$_2$(H)$_2$] Λ-*R*,*R*-Ru2H_2. Photolysis causes reductive elimination of H_2 followed by oxidative addition of H−H, Si−H, B−H, and C−H bonds. The oxidative addition reactions require sterically small substrates such as $PhSiH_3$, C_2H_4, or HBpin. The chiral ligands control the configuration of the stereogenic ruthenium center both in solution as demonstrated by NMR and CD spectroscopy and in the crystalline state such that only a single configuration is formed. However, the particular configuration depends on the nature of the substituent E in *cis*-[Ru(PP*)$_2$(E)(H)] and/or on the mechanism of epimerization at the ruthenium center. All the complexes are stereochemically rigid at room temperature. The CD spectra prove valuable in demonstrating that the complexes are essentially single isomers and in observing several transitions that are typically obscured by overlap within UV/vis absorption spectra. The crystal structures of Δ-*R*,*R*-Ru2(Et_2SiH)(H) and Δ-*R*,*R*-Ru2($PhSiH_2$)(H) show residual Si···$H_{hydride}$ interactions that are absent from their BPE analogues.

The PHIP experiments and the deuterium exchange methods prove a very valuable addition to laser flash photolysis in establishing that the reductive elimination and the readdition of dihydrogen are concerted. The rate constant for reaction of [Ru(DuPHOS)$_2$] with H_2 is slow relative to that for related complexes. Both [Ru(BPE)$_2$] and [Ru(DuPHOS)$_2$] exhibit a kinetic selectivity of H_2 > $PhSiH_3$ > HBpin > Et_2SiH_2, as shown by a combination of transient kinetics and steady state photochemical competition reactions. The photochemical reactions with

dx.doi.org/10.1021/ja210568t | J. Am. Chem. Soc. 2012, 134, 3480−3497

pentafluorobenzene and with ethene constitute the only two C−H activation reactions observed and are distinct from the B−H and Si−H activation reactions. Pentafluorobenzene reacts only with Λ-*R*,*R*-Ru2H_2 and yields a product with a *trans* configuration. The reaction with ethene yields a simple π-complex with Λ-*R*,*R*-Ru2H_2 but a mixture of three products with Λ-*R*,*R*-Ru1H_2, the π-complex, and both the *cis* and *trans* vinyl hydride complexes. The molecular structure of the [Ru(DuPHOS)$_2$] complex with a *trans* configuration shows a significant twist of the RuP_4 skeleton away from square planar, but the *trans*-[Ru(BPE)$_2$] complexes have skeletons close to the ideal D_2 symmetry. We postulate that the twist in the DuPHOS structures acts as the selector that controls the Ru configuration in reaction with substrates.

EXPERIMENTAL SECTION

General Procedures. All operations were performed under a nitrogen or argon atmosphere, either on a high-vacuum line (10^{-4} mbar), on standard Schlenk (10^{-2} mbar) lines, or in a glovebox. Solvents for general use (hexane, cyclohexane, THF, benzene, toluene) were of AR grade, dried by distillation over sodium, and stored under Ar in ampules fitted with a Young's PTFE stopcock. Deuterated solvents were dried by stirring over potassium and distilled under high vacuum into small ampules with a potassium mirror. (*R*,*R*)-Me-BPE, (*R*,*R*)-Me-DuPHOS, (*S*,*S*)-Me-DuPHOS, HBpin, and 2-butanol were obtained from Aldrich. The chiral phosphines are described as of "Kanata purity". [$RuCl_2$(COD)]$_x$ was synthesized according to the literature procedure.[46]

Photochemical reactions at room temperature were performed in pyrex NMR tubes fitted with Young's PTFE stopcocks by using a Philips 125 W medium-pressure mercury vapor lamp with a water filter (5 cm).

Microanalyses were carried out by Elemental Microanalysis Ltd.

NMR Spectroscopy. All standard NMR spectra were recorded on AMX500 spectrometers, unless otherwise stated, in tubes fitted with Young's PTFE stopcocks. All ^{1}H and ^{13}C chemical shifts are reported in ppm (δ) relative to tetramethylsilane and referenced using the chemical shifts of residual protio solvent resonances (benzene, δ 7.16). The ^{31}P{^{1}H} NMR spectra were referenced to external H_3PO_4, ^{11}B NMR spectra to external $BF_3{\cdot}Et_2O$, ^{19}F spectra to external $CFCl_3$, and ^{29}Si spectra to external TMS. 2D NMR spectra were recorded with a standard HMQC pulse program varying the values of cnst2 from 2 to 200 Hz.

In-Situ Photolysis. We described our set up for in situ laser photolysis within an NMR spectrometer in recent papers.[34] Laser photolysis was carried out with a pulsed Nd:YAG laser (Continuum Surelite II) fitted with a frequency tripling crystal. Operating conditions were typically 10 Hz repetition rate, flash lamp voltage 1.49 kV, Q-switch delay increased from the standard to 320 μs, yielding a laser power of 85 mW when operating at 355 nm. A very dilute sample of [Ru(CO)$_2$($Ph_2PCH_2CH_2PPh_2$)(PPh_3)] in C_6D_6 was used for laser alignment, with *para*-hydrogen amplification in real time. NMR spectra were recorded on a Bruker Avance wide-bore 600 MHz spectrometer. For PHIP experiments, hydrogen enriched in the para spin state was prepared by cooling H_2 to 35 K over activated charcoal using the system described previously.[47]

Laser Flash Photolysis. Samples were prepared exclusively in the glovebox. They were loaded into a quartz cuvette (10 mm pathlength) fitted with a Young's PTFE stopcock, a degassing bulb, and a greaseless Young's connection. The complex (ca. 2−3 mg) was dissolved in cyclohexane (5 mL) in an argon-filled glovebox with a concentration selected to have an absorbance at the laser wavelength (308 nm) between 0.6 and 0.85. Liquid quenchers were added with a microliter syringe to the solution containing the complexes. The solution was then degassed by freeze−pump−thaw cycle (3 times) on a high-vacuum Schlenk line before being backfilled with the appropriate gas. The gaseous quencher (or argon) was admitted up to 1 atm pressure on the high vacuum Schlenk line. For high pressure work the window edges of the cuvette were flamed to secure the seal and the Young's connection was replaced by a glass-to-metal seal and a Swagelok fitting. The gas was admitted on a high pressure line and the pressure measured with an MKS Baratron capacitance manometer. The cell was held in a metal container for safety. A single sample was used for each run with increasing gas pressure. The results were consistent with a corresponding run with decreasing gas pressure. The variable pressure measurements were performed on two different samples each for H_2 and D_2 and were carried out side-by-side on the same day. The gases were of Research grade: deuterium 99.96 atom % D, Isotec; hydrogen N5.5, BOC; argon N5.5, BOC.

The apparatus consists of an excimer laser (MPB Technologies Inc., MSX-250) operating at 308 nm (XeCl) as the exciting source, coupled to an Applied Photophysics laser kinetic spectrometer with a Xe arc lamp (XM-300-5 HS made by ORC) as a white light source. The laser pulse (ca. 11 ns) is focused into a beam of ca. 1-mm diameter and directed through the sample together with the monitoring beam in a collinear arrangement by means of a quartz beam splitter. Light falling on the photomultiplier detector is sampled by a Tektronix TDS 520 oscilloscope and transferred to a computer for data analysis and storage. Transient decays are usually analyzed as 15 shot averages. The computer is used to fire the laser, and the oscilloscope is triggered by diverting part of the laser beam and focusing onto a photodiode. Transient spectra are obtained by the point-by-point method and correspond to difference spectra after particular fixed times following the laser flash. The samples were maintained at 295 K.

Mass Spectra. EI mass spectra and the LIFDI mass spectra were measured on a Waters Micromass GCT Premier orthogonal time-of-flight instrument set to one scan per second with resolution power of 6000 fwhm and equipped with a LIFDI probe from LINDEN GmbH. The design is very similar to that described by Gross et al.[48] Toluene was used for tuning the instrument. The polyethylene glycol probe was kept at ambient temperature with the emitter potential at 12 kV. Activated tungsten wire LIFDI emitters (13 μm tungsten from LINDEN) were ramped manually up to 100 mA for the emitter heating current during the experiment.

UV/Vis Absorption and Circular Dichroism. CD spectra were run on a Jasco J-810 spectropolarimeter at room temperature (20 °C) from 550 to 215 nm with a speed of 200 nm/min in a 1 cm cuvette fitted with a Young's PTFE stopcock. The same solutions were used for UV/vis spectroscopy (UV/vis ChemStation Agilent 8453). Samples derived from Δ-*S*,*S*-Ru2H_2 and Λ-*R*,*R*-Ru2H_2 were diluted to match their UV absorbances. The CD and UV/vis spectra were recorded on the same day for each sample. The contribution of the solvent was subtracted and data analyzed with Microcal Origin 6.1. Values of $\Delta\varepsilon$ were calculated using the equation $\Delta\varepsilon = \theta/(32982 \times c \times l)$, where θ is ellipticity in mdeg, c is the concentration in mol dm^{-3}, and l is the path length in cm.[49] UV/vis and CD data are listed in the Supporting Information.

X-ray Crystallography. Crystallographic parameters are summarized in Tables 5 and 6. Diffraction data for Λ-*R*,*R*-Ru1H_2, Λ-*R*,*R*-Ru2H_2, Λ-*R*,*R*-Ru1(Et_2SiH)(H), and Δ-*R*,*R*-Ru2(η^2-C_2H_4) were collected at 110 K on a Bruker Smart Apex diffractometer with Mo Kα radiation (λ = 0.71073 Å) using a SMART CCD camera. Diffractometer control, data collection, and initial unit cell determination was performed using SMART (v5.625 Bruker-AXS). Frame integration and unit-cell refinement was carried out with SAINT+ (v6.22, Bruker AXS). Absorption corrections were applied using SADABS (v2.03, Sheldrick). The structures were solved by either Patterson or direct methods using SHELXS-97 (Sheldrick, 1997) and refined by full-matrix least-squares using SHELXL-97 (Sheldrick, 1997).[50] Diffraction data for Δ-*S*,*S*-Ru2H_2, Δ-*R*,*R*-Ru2(Et_2SiH)(H), Λ-*R*,*R*-Ru1($PhSiH_2$)(H), Δ-*R*,*R*-Ru2($PhSiH_2$)(H), Λ-*R*,*R*-Ru1(Bpin)(H), Λ-*S*,*S*-Ru2(η^2-C_2H_4), *trans*-*R*,*R*-Ru2(C_6F_5)(H), *trans*-*R*,*R*-Ru1Cl_2, and *trans*-*R*,*R*-Ru1(Br)(H) were collected at 110 K on an Agilent SuperNova diffractometer with Mo Kα radiation (λ = 0.71073 Å). Data collection, unit cell determination, and frame integration were carried out with "CrysalisPro". Absorption corrections were applied using crystal face-indexing and the ABSPACK absorption correction software within CrysalisPro. Structures were solved and refined using Olex2[51] implementing SHELX algorithms. Structures were solved by either Patterson or direct methods using SHELXS-97

Table 5. Crystallographic Data for Λ-*R*,*R*-Ru1H$_2$, Δ-*S*,*S*-Ru2H$_2$, Λ-*R*,*R*-Ru2H$_2$, Λ-*R*,*R*-Ru1(Et$_2$SiH)(H), Λ-*R*,*R*-Ru1(PhSiH$_2$)(H), Δ-*R*,*R*-Ru2(Et$_2$SiH)(H), and Δ-*R*,*R*-Ru2(PhSiH$_2$)(H)

	Λ-*R*,*R*-Ru1H$_2$	Δ-*S*,*S*-Ru2H$_2$·hexane	Λ-*R*,*R*-Ru2H$_2$·hexane	Λ-*R*,*R*-Ru1(Et$_2$SiH)(H)	Λ-*R*,*R*-Ru1(PhSiH$_2$)(H)	Δ-*R*,*R*-Ru2(Et$_2$SiH)(H)	Δ-*R*,*R*-Ru2(PhSiH$_2$)(H)
formula	$C_{28}H_{58}P_4Ru$	$C_{42}H_{72}P_4Ru$	$C_{42}H_{72}P_4Ru$	$C_{32}H_{68}P_4RuSi$	$C_{34}H_{64}P_4RuSi$	$C_{40}H_{68}P_4RuSi$	$C_{42}H_{64}P_4RuSi$
formula weight	619.69	801.95	801.95	705.90	725.89	801.98	821.97
T/K	110(2)	110(2)	110(2)	110(2)	110(2)	110(2)	110(2)
crystal system	trigonal	orthorhombic	orthorhombic	monoclinic	orthorhombic	monoclinic	monoclinic
space group	$P3_2$	$P2_12_12_1$	$P2_12_12_1$	$P2_1$	$P2_12_12_1$	$P2_1$	$P2_1$
a (Å)	10.5462(3)	10.4162(13)	10.4095(13	10.7597(6)	10.8954(6)	11.2756(4)	11.6044(3)
b (Å)	10.5462(3)	14.9533(9)	14.9482(19)	17.1350(10)	18.2414(9)	17.8651(5)	16.5646(2)
c (Å)	24.2854(16)	26.769(11)	26.671(3)	20.2240(11)	18.2696(9)	11.2779(5)	12.0137(3)
α (deg)	90	90	90	90	90	90	90
β (deg)	90	90	90	105.1160(10)	90	116.017(5)	118.031(3)
γ (deg)	120	90	90	90	90	90	90
V/Å^3	2339.20(18)	4169.4(18)	4150.1(9)	3599.6(4)	3631.0(3)	2041.59(13)	2038.40(8)
Z	3	4	4	4	4	2	2
ρ_{calc} (mg/m^3)	1.320	1.278	1.284	1.303	1.328	1.305	1.339
F(000)	990	1712	1712	1512	1544	852	868
reflns collected	35612	14373	42415	41336	20656	6280	18668
ind reflns	9030	8493	10321	20034	8153	5671	11806
data/restraints/parameters	9030/28/376	8493/1/442	10321/0/442	20034/17/737	8153/0/379	5671/1/433	11806/1/453
GooF on F^2	1.056	1.093	1.155	1.034	1.049	1.055	1.015
R_1 [$I > 2\sigma(I)$]	0.0268	0.0452	0.0276	0.0309	0.0275	0.0307	0.0273
$wR2$ (all data)	$wR2$ = 0.0595	$wR2$ = 0.1090	$wR2$ = 0.0675	$wR2$ = 0.0673	$wR2$ = 0.0578	$wR2$ = 0.0805	$wR2$ = 0.0600
max. diff peak and hole (e Å^{-3})	0.813, −0.707	1.054, − 0.752	0.972, −0.334	1.076, −0.407	0.383, −0.267	0.710, −0.531	0.391, −0.275
absolute structure (Flack)	−0.012(17)	0.01(3)	−0.005(18)	−0.034(12)	−0.025(18)	−0.04(3)	−0.047(13)
CCDC no.	853298	853300	853299	853301	853302	853303	853304

Table 6. Crystallographic Data for Λ-*R*,*R*-Ru1(Bpin)(H), Λ-*S*,*S*-Ru2(η^2-C$_2$H$_4$), Δ-*R*,*R*-Ru2(η^2-C$_2$H$_4$), *trans*-*R*,*R*-Ru2(C$_6$F$_5$)(H), *trans*-*R*,*R*-Ru1(Br)(H), and *trans*-*R*,*R*-Ru1(Cl)$_2$

	Λ-*R*,*R*-Ru1(Bpin)(H)	Λ-*S*,*S*-Ru2(η^2-C$_2$H$_4$)	Δ-*R*,*R*-Ru2(η^2-C$_2$H$_4$)	*trans*-*R*,*R*-Ru2(C$_6$F$_5$)(H)	*trans*-*R*,*R*-Ru1(Br)(H)	*trans*-*R*,*R*-Ru1(Cl)$_2$
formula	$C_{34}H_{69}BO_2P_4Ru$	$C_{38}H_{60}P_4Ru$	$C_{38}H_{60}P_4Ru$	$C_{42}H_{57}F_5P_4Ru$	$C_{28}H_{57}BrP_4Ru$	$C_{28}H_{56}Cl_2P_4Ru$
formula weight	745.65	741.81	741.81	881.83	698.60	688.58
T/K	110(2)	110(2)	110(2)	110(2)	110(2)	110(2)
cryst syst	orthorhombic	orthorhombic	orthorhombic	monoclinic	triclinic	orthorhombic
space group	$P2_12_12_1$	$P2_12_12_1$	$P2_12_12_1$	$P2_1$	$P1$	$P2_12_12_1$
a (Å)	10.09766(17)	10.2481(3)	10.2545(14)	12.52495(14)	9.666(3)	11.60235(14)
b (Å)	18.0979(3)	17.7037(5)	17.707(2)	12.65101(13)	11.403(2)	13.80119(14)
c (Å)	20.9211(3)	19.8698(5)	19.889(3)	12.52993(13)	15.665(4)	19.8946(2)
α (deg)	90	90	90	90	73.02(2)	90
β (deg)	90	90	90	92.9129(10)	89.56(2)	90
γ (deg)	90	90	90	90	75.84(2)	90
V/Å^3	3823.25(10)	3604.96(16)	3611.3(8)	1982.84(4)	1597.4(7)	3185.65(6)
Z	4	4	4	2	2	4
ρ_{calc} (mg/m^3)	1.295	1.367	1.364	1.477	1.452	1.436
F(000)	1592	1568	1568	961	728	1448
reflns collected	31688	33778	49507	14233	13356	16563
ind reflns	10702	11534	8955	8822	9568	8917
data/restraints/parameters	10702/0/395	11534/0/412	8955/0/412	8822/1/481	9568/3/637	8917/0/324
GooF on F^2	1.055	1.058	1.049	1.035	1.016	1.014
R_1 [$I > 2\sigma(I)$]	0.0249	0.0251	0.0242	0.0257	0.0296	0.0317
$wR2$ (all data)	0.0540	0.0538	0.0562	0.0541	0.0551	0.0576
max. diff peak and hole (e Å^{-3})	0.530, −0.270	0.541, −0.300	0.641, −0.219	0.410, −0.360	0.565, −0.451	0.477, −0.383
absolute structure (Flack)	−0.040(13)	−0.034(13)	−0.007(15)	−0.068(14)	−0.001(5)	−0.022(19)
CCDC no.	853305	853306	853307	853308	853310	853309

and refined by full-matrix least-squares using SHELXL-97.[50] All non-hydrogen atoms were refined anisotropically. Carbon-bound hydrogen atoms were placed at calculated positions and refined using a "riding model". Hydrogen atoms bound to ruthenium, silicon, and also for coordinated ethene were found by difference map and refined.

dx.doi.org/10.1021/ja210568t | J. Am. Chem. Soc. 2012, 134, 3480−3497

Syntheses and NMR Experiments. [Ru(PP*)$_2$(H)$_2$]. The complexes were synthesized by heating with stirring [Ru(COD)Cl$_2$]$_x$, the corresponding bidentate phosphine, and NaOH in 2-butanol at 80 °C, in a similar manner to the literature procedure. Instead of 3 h of heating, the reaction was run overnight.[19] In cases where the value of J_{HH} is given after a multiplet designation, this value was measured from ^{1}H{^{31}P} spectra and J_{PH} was not determined. The following superscript abbreviations are used: ^{r} denotes ring of the phospholane, ^{b} backbone, ^{e} ethylene, ^{Si} silane, ^{R} and ^{S} enantiomers.

Λ-[*cis*-Ru((*R*,*R*)-Me-BPE)$_2$(H)$_2$], Λ-*R*,*R*-Ru1H$_2$ (C$_6$D$_6$, 300 K), ^{1}H: δ 2.09 (m, 2H, CH$_2^r$), 1.95 (m, 4H, 2CH$_2^r$ and 2CH), 1.87 (m, 2H, CH$_2^b$), 1.68 (m, 6H, CH), 1.53 (q, J_{PH} = 15.8, J_{HH} = 6.9 Hz, 6H, CH$_3$), 1.44 (m, 2H, CH$_2^r$), 1.38 (m, 2H, CH$_2^r$), 1.23 (m, 2H, CH$_2^r$), 1.16 (dd, J_{PH} = 12.8, J_{HH} = 7.1 Hz, 6H, CH$_3$), 1.12 (dd, J_{PH} = 16.4, J_{HH} = 7.4 Hz, 6H, CH$_3$), 1.02 (q, J_{PH} = 11.8, J_{HH} = 6.7 Hz, 6H, CH$_3$), 0.8 (m, 3H, CH$_2^b$), 0.68 (m, 3H, CH$_2^b$), −10.7 (m, Ru−H); ^{31}P{^{1}H}: δ 101.5 (t, J_{PP} = 17 Hz), 96.8 (t, J_{PP} = 17 Hz); ^{13}C{^{1}H}: δ 39.47 (m, CH), 39.34 (m, CH), 38.15 (m, CH), 33.44, 34.4, 35.02, 35.76 (s, CH$_2^r$), 28.85 (m, CH$_2^b$), 28.13 (q, J_{PC} = 15 Hz, CH$_2^b$), 21.86 (t, J_{PC} = 5 Hz, CH$_3$), 21.22 (t, J_{PC} = 8 Hz, CH$_3$), 15.54 (s, CH$_3$), 14.12 (s, CH$_3$). gNMR simulation values for ^{1}H resonance at δ −10.7: *trans*-J_{PP} = 68 Hz, *cis*-J_{PP} = −25 and 25 Hz, J_{HH} = 3.5 Hz. ^{31}P{^{1}H}: *trans*-J_{PP} = 200 Hz, *cis*-J_{PP} = 17 and 4.7 Hz. Anal. Calcd for C$_{28}$H$_{58}$P$_4$Ru (619.69 g·mol^{-1}) C, 54.27; H, 9.43. Found: C, 54.00; H, 9.44. IR (hexane, cm^{-1}): 1835. Mass spectra (EI, *m*/*z*): 618 (100%, [M − H$_2$]$^+$); (LIFDI, *m*/*z*): 620 (70%, M$^+$), 618 (100%, [M − H$_2$]$^+$), exp 620.2404, calcd for C$_{28}$H$_{58}$P$_4$Ru 620.2533, difference −12.5 mDa.

Δ-[*cis*-Ru((*S*,*S*)-Me-DuPHOS)$_2$(H)$_2$], Δ-*S*,*S*-Ru2H$_2$, or Λ-[*cis*-Ru-((*R*,*R*)-Me-DuPHOS)$_2$(H)$_2$], Λ-*R*,*R*-Ru2H$_2$ (C$_6$D$_6$, 300 K), ^{1}H: δ 7.64 (d, J_{HH} = 7 Hz, 2H, Ph), 7.52 (d, J_{HH} = 7 Hz, 2H, Ph), 7.11 (d, J_{HH} = 7 Hz, 4H, Ph), 2.62 (m, 4H, CH, CH$_2$), 2.42 (m, 2H, CH), 2.16 (m, 6H, CH, CH$_2$), 1.85 (m, 6H, CH, CH$_2$), 1.66 (q, 6H, J_{PH} = 17, J_{HH} = 7 Hz, 6H, CH$_3$), 1.56 (m, 4H, CH$_2$), 1.33 (m, 2H, CH$_2$), 1.04 (q, 6H, J_{PH} = 15, J_{HH} = 7 Hz, 6H, CH$_3$), 0.87 (dd, 6H, J_{PH} = 17, J_{HH} = 7 Hz, 6H, CH$_3$), 0.60 (dd, 6H, J_{PH} = 13, J_{HH} = 7 Hz, 6H, CH$_3$), −10.0 (m, 2H, Ru−H); ^{31}P{^{1}H}: δ 103.35 (t, J_{PP} = 20 Hz), 100.12 (t, J_{PP} = 20 Hz); ^{13}C{^{1}H}: δ 152.33 (m, C^b), 147.02 (m, C^b), 131.3 (m, J_{PC} = 7 Hz, CH^b), 129.57 (t, J_{PC} = 8 Hz, CH^b), 127.66 (s, CH^b), 127.24 (s, CH^b), 45.77 (m, J_{PC} = 11 Hz, CH), 43.18 (m, J_{PC} = 11 Hz, CH), 40.21 (m, J_{PC} = 16 Hz, CH), 37.52 (s, CH$_2$), 36.82 (s, CH$_2$), 35.45 (m, CH, CH$_2$), 35.08 (s, CH$_2$), 26.14 (s, CH$_2$), 21, 94 (m, CH$_3$), 21.78 (s, CH$_3$), 17.15 (s, CH$_3$), 13.76 (s, CH$_3$). gNMR simulation values for ^{1}H resonance at δ −10: *trans*-J_{PH} = 71 Hz, *cis*-J_{PH} = 25.5 and −19.5 Hz, J_{HH} = 6.5 Hz. ^{31}P{^{1}H}: *trans*-J_{PP} = 200 Hz, *cis*-J_{PP} = 7 and 20 Hz. Anal. Calcd for C$_{36}$H$_{58}$P$_4$Ru (716.25 g·mol^{-1}) C, 60.40; H, 8.17. Found: C, 59.87; H, 8.33. IR (hexane, cm^{-1}): 1845. Mass spectra (EI, *m*/*z*): 714 (100%, [M − H$_2$]$^+$); (LIFDI, *m*/*z*): 716 (60%, M$^+$), 714 (100%, [M − H$_2$]$^+$), exp 716.2469, calcd for C$_{36}$H$_{58}$P$_4$Ru 716.2533, difference −6.4 mDa.

Λ-[*cis*-Ru((*R*,*R*)-Me-BPE)$_2$(Et$_2$SiH)(H)], Λ-*R*,*R*-Ru1(Et$_2$SiH)(H). An NMR tube was charged with Λ-*R*,*R*-Ru1H$_2$ (∼ 5 mg) and a slight excess of Et$_2$SiH$_2$ in hexane; the solution was degassed and then irradiated with UV light. The solution remains colorless. The progress of the reaction was followed by ^{31}P NMR spectroscopy. Reactions performed in hexane or C$_6$D$_6$ or neat silane produced the same results. NMR (C$_6$D$_6$, 300 K), ^{1}H: δ 3.99 (br, 1H, H^{Si}), 2.64 (m, J_{HH} = 7 Hz, 1H, CH$_2^b$), 2.42 (m, J_{HH} = 6 Hz, 2H, CH$_2^r$), 2.31 (m, J_{HH} = 7 Hz, 1H, CH$_2^r$), 2.15 (m, J_{HH} = 7 Hz, 1H, CH), 2.05 (m, J_{HH} = 7 Hz, 3H, CH, CH$_2^r$), 1.90 (m, J_{HH} = 6 Hz, 5H, CH, CH$_2^r$), 1.73 (m, J_{HH} = 8 Hz, 2H, CH), 1.62 (m, J_{HH} = 8 Hz, 6H, CH$_3^{Si}$), 1.43 (m, J_{HH} = 8 Hz, 6H, CH$_3$, CH$_2^{Si}$), 1.25 (dd, J_{HH} = 7, J_{PH} = 11 Hz, 3H, CH$_3$), 1.19 (dd, J_{HH} = 7, J_{PH} = 12 Hz, 3H, CH$_3$), 1.04 (m, J_{HH} = 7 Hz, 4H, CH, CH$_3$), 0.91 (overlapping dd, J_{HH} = 7, J_{PH} = 10 Hz, 9H, 3CH$_3$), 0.67 (m, 6H, CH$_2^b$, CH$_2^{Si}$), −10.04 (m, 1H, Ru−H); ^{31}P{^{1}H}: δ_A 104.9 (ddd, J_{AX} = 224, J_{AM} = J_{AQ} = 25 Hz), δ_M 90.52 (pseudoq, J_{MA} = 25, J_{MQ} = J_{MX} = 21 Hz, P$_{transH}$), δ_Q 88.03 (m, J_{QA} = 25, J_{QM} = J_{QX} = 21 Hz, P$_{transSi}$), δ_X 82.11 (dt, J_{XA} = 224, J_{XM} = J_{XQ} = 21 Hz); ^{1}H−^{29}Si HMQC: δ 23.42 (dd, J_{SiH} =146 Hz, J_{SiP} =138 Hz), ^{1}H−^{29}Si{^{31}P} HMQC: δ 23.42 d, $J_{SiHhydride}$ = 8 Hz. gNMR simulation values for ^{1}H resonance at δ −10.04: *trans*-J_{PH} = 65 Hz, *cis*-J_{PH} = −26, −19.5, and −21 Hz. ^{31}P{^{1}H}: *trans*-J_{PP} = 224 Hz, *cis*-J_{PP} = 21 and 25 Hz.

Λ-[*cis*-Ru((*S*,*S*)-Me-DuPHOS)$_2$(Et$_2$SiH)(H)], Λ-*S*,*S*-Ru2(Et$_2$SiH)-(H) or Δ-[*cis*-Ru((*R*,*R*)-Me-DuPHOS)$_2$(Et$_2$SiH)(H)], Δ-*R*,*R*-Ru2-(Et$_2$SiH)(H). A similar procedure was followed, resulting in a yellow/orange solution. NMR (C$_6$D$_6$, 300 K), ^{1}H: δ 7.75−6.89 (8H, Ph), 4.38 (br, 1H, H^{Si}), 2.80 (m, 2H, CH$_2$), 2.61 (m, 2H, CH), 2.41 (m, 2H, CH$_2$), 2.23 (m, 2H, CH$_2$), 2 (m, 1H, CH), 1.79 (t, J_{HH} = 8 Hz, 6H, 2CH$_3^{Si}$), 1.53 (dd, J_{PH} = 12, J_{HH} = 7 Hz, 6H, 2CH$_3$), 1.49 (m, 4H, CH$_2^{Si}$), 0.28 (dd, J_{PH} = 12, J_{HH} = 7 Hz, 3H, CH$_3$), 0.22 (dd, J_{PH} = 12, J_{HH} = 7 Hz, 3H, CH$_3$), 0.11 (dd, J_{PH} = 12, J_{HH} = 7 Hz, 3H, CH$_3$), −9.5 (m, 1H, Ru−H); ^{31}P{^{1}H}: δ_A 102.3 (ddd, J_{AX} = 228, J_{AM} = J_{AQ} = 19 Hz), δ_X 98.63 (dt, J_{XA} = 228, J_{XM} = J_{XQ} = 25 Hz), δ_M 71.34 (q, J_{MA} = J_{MX} = 25, J_{MQ} = 19 Hz, P$_{transH}$), δ_Q 63.38 (m, J_{QM} = J_{QX} = 25, J_{QA} = 19 Hz, P$_{transSi}$); ^{1}H−^{29}Si HMQC: δ 10.8 (dd, J_{SiH} = 141 Hz, J_{SiP} = 132 Hz). Anal. Calcd for C$_{40}$H$_{68}$P$_4$RuSi (802.31 g·mol^{-1}) C, 59.9; H, 8.55. Found: C, 59.04; H, 8.06. Mass spectra (LIFDI, *m*/*z*): 714 (100%, [M−H$_2$]$^+$), 802 (45%, M$^+$), exp 802.3100, calcd for C$_{40}$H$_{68}$P$_4$RuSi 802.3084, difference 1.6 mDa.

Λ-[*cis*-Ru((*R*,*R*)-Me-BPE)$_2$(PhSiH$_2$)(H)], Λ-*R*,*R*-Ru1(PhSiH$_2$)(H). A similar procedure was followed, resulting in a slight yellow solution. NMR (C$_6$D$_6$, 300 K), ^{1}H: δ 8.25 (d, J_{HH} = 7 Hz, 2H, Ph^{Si}), 7.30 (t, J_{HH} = 7 Hz, 2H, Ph^{Si}), 7.21 (t, J_{HH} = 7 Hz, 1H, Ph^{Si}), 4.86 (pseudoq, J_{PH} = 20, J_{HH} = 7 Hz, 1H, H^{Si}), 4.56 (m, J_{PH} = 20, J_{HH} = 7 Hz, 1H, H^{Si}), 2.68 (m, J_{HH} = 7 Hz, 2H, CH$_2^b$), 2.38 (m, J_{HH} = 7 Hz, 1H, CH$_2^r$), 2.06 (m, 2H, CH, CH$_2^r$), 1.94 (m, 4H, CH, CH$_2^r$), 1.77 (m, 3H, CH), 1.66 (m, 2H, CH), 1.54 (dd, J_{PH} = 16, J_{HH} = 7 Hz, 6H, 2CH$_3$), 1.46 (dd, J_{PH} = 12, J_{HH} = 7 Hz, 3H, CH$_3$), 1.36 (m, 4H, CH, CH$_2^r$), 1.25 (m, 10H, CH, CH$_2^b$, CH$_3$), 1.09 (dd, J_{PH} = 12, J_{HH} = 7 Hz, 3H, CH$_3$), 0.96, 0.91 (overlapping dd, J_{PH} = 16, J_{HH} = 7 Hz, 9H, 3CH$_3$), 0.85 (dd, J_{PH} = 12, J_{HH} = 7 Hz, 3H, CH$_3$), −9.91 (m, 1H, Ru−H); ^{31}P{^{1}H}: δ_A 101.16 (ddd, J_{AX} = 222, J_{AM} = J_{AQ} = 25 Hz), δ_M 92.13 (q, J_{MA} = J_{MX} = 25, J_{MQ} = 19 Hz, P$_{transH}$), δ_Q 85.87 (q, J_{QA} = 20, J_{QM} = J_{QX} = 17 Hz, P$_{transSi}$), δ_X 84.58 (dt, J_{XA} = 223, J_{XM} = J_{XQ} = 20 Hz); ^{1}H−^{29}Si HMQC: δ −18.17 (dd, J_{SiH} =146 Hz, J_{SiP} =163 Hz), ^{1}H−^{29}Si{^{31}P} HMQC: δ −18.17 d, $J_{SiHhydride}$ = 8 Hz.

Δ-[*cis*-Ru((*R*,*R*)-Me-DuPHOS)$_2$(PhSiH$_2$)(H)], Δ-*R*,*R*-Ru2(PhSiH$_2$)(H). A similar procedure was followed, resulting in a yellow solution. NMR (C$_6$D$_6$, 300 K), ^{1}H: δ 8.46 (d, J_{HH} = 7 Hz, 2H, Ph^{Si}), 7.39 (t, J_{HH} = 7 Hz, 2H, Ph^{Si}), 7.27 (m, 4H, Ph^{Si}, Ph), 7.07 (m, 3H, Ph^{Si}, Ph), 6.89 (dd, J_{HH} = 7, 20 Hz, 4H, Ph^{Si}, Ph), 5.62 (m, 1H, H^{Si}), 5.47 (br d, J_{HH} = 6 Hz, 1H, H^{Si}), 3.12 (m, J_{HH} = 7 Hz, 1H, CH$_2$), 2.71 (m, J_{HH} = 7 Hz, 1H, CH$_2$), 2.53 (m, J_{HH} = 7 Hz, 2H, CH$_2$), 2.35 (m, J_{HH} = 7 Hz, 1H, CH), 2.2 (m, J_{HH} = 7 Hz, 1H, CH), 2.06 (m, J_{HH} = 7 Hz, 1H, CH), 1.96 (m, J_{HH} = 7 Hz, 2H, CH, CH$_2$), 1.86 (dd, J_{HH} = 7, J_{PH} = 16 Hz, 3H, CH$_3$), 1.79 (m, J_{HH} = 7 Hz, 2H, CH, CH$_2$), 1.71 (dd, J_{HH} = 7, J_{PH} = 17 Hz, 3H, CH$_3$), 1.63 (m, J_{HH} = 7 Hz, 3H, 2CH, CH$_2$), 1.56 (dd, J_{HH} = 7, J_{PH} = 16 Hz, 3H, CH$_3$), 1.37 (m, J_{HH} = 7 Hz, 5H, 3CH, 2CH$_2$), 1.19 (dd, J_{HH} = 7, J_{PH} = 17 Hz, 3H, CH$_3$), 0.28 (dd, J_{HH} = 7, J_{PH} = 12 Hz, 3H, CH$_3$), 0.21 (overlapping dd, 6H, 2CH$_3$), 0.15 (dd, J_{HH} = 7, J_{PH} = 12 Hz, 3H, CH$_3$), −9.11 (m, 1H, Ru−H); ^{31}P{^{1}H}: δ_A 101.88 (ddd, J_{AX} = 221, J_{AM} = J_{AQ} = 21 Hz), δ_X 96.12 (dt, J_{XA} = 221, J_{XM} = J_{XQ} = 26 Hz), δ_M 73.61 (q, J_{MA} = J_{MX} = 25, J_{MQ} = 20 Hz, P$_{transH}$), δ_Q 60.82 (m, J_{QA} = 20, J_{QM} = J_{QX} = 26 Hz, P$_{transSi}$); ^{1}H−^{29}Si HMQC: δ −23.91 (dd, J_{SiH} =147 Hz, J_{SiP} =159 Hz). Anal. Calcd for C$_{42}$H$_{64}$P$_4$RuSi (822.28 g·mol^{-1}) C, 61.37; H, 7.85. Found: C, 61.83; H, 7.81. Mass spectra (LIFDI, *m*/*z*): 822 (30%, M$^+$), 714 (100%, [M − H$_2$]$^+$).

Λ-[*cis*-Ru((*R*,*R*)-Me-BPE)$_2$(MePhSiH)(H)], Λ-*R*,*R*-Ru1-(MePhSi^{R}H)(H): Λ-*R*,*R*-Ru1(MePhSi^{S}H)(H) mixture, ratio 2:1 (the identification of Si^R and Si^S is arbitrary). A similar procedure was followed, resulting in a yellow solution. Selected NMR (C$_6$D$_6$, 300 K), ^{1}H: δ^R 8.32 (d, J_{HH} = 7 Hz, 1H, Ph^{Si}), δ^S 8.24 (d, J_{HH} = 7 Hz, 2H, Ph^{Si}), 7.3−7.0 (m, Ph^{Si}, Ph), δ^R 5.1 (m, 1H, H^{Si}), δ^S 4.9 (m, 1H, H^{Si}), δ^R −9.6 (m, 1H, Ru−H), δ^S −9.8 (m, 1H, Ru−H); ^{31}P{^{1}H}: $\delta_A{}^R$ 103.2 (ddd, J_{AX} = 222, J_{AM} = J_{AQ} = 26 Hz), $\delta_A{}^S$ 103.1 (ddd, J_{AX} = 222, J_{AM} = J_{AQ} = 26 Hz), $\delta_M{}^S$ 90.3 (m, J_{MA} = J_{MX} = 26, J_{MQ} = 21 Hz, P$_{transH}$), $\delta_M{}^R$ 89.9 (m, J_{MA} = J_{MX} = 26, J_{MQ} = 21 Hz, P$_{transH}$), $\delta_Q{}^R$ 88.4 (m, J_{QA} = 26, J_{QM} = J_{QX} = 21 Hz, P$_{transSi}$), $\delta_Q{}^S$ 83.9 (m, J_{QA} = 26, J_{QM} = J_{QX} = 21 Hz, P$_{transSi}$), $\delta_X{}^R$ 81.1 (dt, J_{XA} = 222, J_{XM} = J_{XQ} = 21 Hz), $\delta_X{}^S$ 80.7 (dt, J_{XA} = 222, J_{XM} = J_{XQ} = 21 Hz).

Δ-[*cis*-Ru((*R*,*R*)-Me-DuPHOS)$_2$(MePhSiH)(H)], Δ-*R*,*R*-Ru2(MePhSi^{R}H)(H): Δ-*R*,*R*-Ru2(MePhSi^{S}H)(H) mixture, ratio 1:1

(the identifications of Si^R, Si^S, Λ-Ru, and Δ-Ru are arbitrary). A similar procedure was followed resulting in a yellow solution. Selected NMR (C_6D_6, 300 K), ^{1}H: δ^R 8.31 (d, J_{HH} = 7 Hz, 2H, Ph^{Si}), δ^S 8.23 (d, J_{HH} = 7 Hz, 2H, Ph^{Si}), 7.47−6.8 (m, Ph^{Si}, Ph), δ^R 5.6 (m, 1H, H^{Si}), δ^S 5.5 (m, 1H, H^{Si}), δ^R −9.13 (m, 1H, Ru−H), δ^S −9.25 (m, 1H, Ru−H); ^{31}P{^{1}H}: $\delta_A{}^R$ 102.3 (ddd, J_{AX} = 225, J_{AM} = J_{AQ} = 33 Hz), $\delta_A{}^S$ 101.2 (ddd, J_{AX} = 225, J_{AM} = J_{AQ} = 33 Hz), $\delta_X{}^R$ 96.6 (dt, J_{XA} = 225, J_{XM} = J_{XQ} = 25 Hz), $\delta_X{}^S$ 95.2 (dt, J_{XA} = 225, J_{XM} = J_{XQ} = 25 Hz), $\delta_M{}^R$ 72.9 (q, J_{MA} = J_{MX} = 33, J_{MQ} = 25 Hz, P_{transH}), $\delta_M{}^S$ 71.9 (q, J_{MA} = J_{MX} = 33, J_{MQ} = 25 Hz, P_{transH}), 62.8 $\delta_Q{}^R$ (m, J_{QA} = 33, J_{QM} = J_{QX} = 25 Hz, $P_{transSi}$), $\delta_Q{}^S$ 60.0 (m, J_{QA} = 33, J_{QM} = J_{QX} = 25 Hz, $P_{transSi}$).

Λ-[Ru((*R*,*R*)-Me-BPE)$_2$(C_2H_4)], Λ-*R*,*R*-Ru1(η^2-C_2H_4), *cis*- and *trans*-[Ru((*R*,*R*)-Me-BPE)$_2$(C_2H_3)(H)], *cis*-/*trans*-*R*,*R*-Ru1(C_2H_3)-(H). An NMR tube was charged with Λ-*R*,*R*-Ru1H_2 (∼5 mg) and C_6D_6, the solution was degassed, and then C_2H_4 (1 atm) was added. The solution was irradiated with UV light for 1 h. The products were not separated. *trans*-*R*,*R*-Ru1(C_2H_3)(H) NMR (C_6D_6, 300 K), ^{1}H: δ 8.37 (m, J_{HH} = 20, 13 Hz, 1H, CH^e), 6.78 (dd, J_{HH} = 13, 6 Hz, 1H, CH^e), 5.67 (dd, J_{HH} = 20, 6 Hz, 1H, CH^e), −12.27 (quin, J_{PH} = 22 Hz, 1H, Ru−H); ^{31}P{^{1}H}: δ 89.31 (t, J_{PP} = 28 Hz), 80.3 (t, J_{PP} = 28 Hz); *cis*-*R*,*R*-Ru1(C_2H_3)(H) NMR (C_6D_6, 300 K), ^{1}H: δ 7.53 (m, J_{HH} = 20, 5 Hz, 1H, CH^e), 6.58 (m, J_{HH} = 12, 6 Hz, 1H, CH^e), 5.67 (dd, J_{HH} = 20, 6 Hz, 1H, CH^e), −8.93 (dq, J_{PH} = 25, 20 Hz, 1H, Ru−H); Λ-*R*,*R*-Ru1(η^2-C_2H_4) NMR (C_6D_6, 300 K), ^{1}H: δ 2.06 (m, 2H, $CH_2{}^r$), 1.96 (m, 4H, $2CH_2{}^r$ and 2CH), 1.85 (m, 2H, $CH_2{}^b$), 1.65 (m, 3H, CH, $CH_2{}^e$), 1.48 (m, J_{PH} = 8, 7.2 Hz, 6H, CH_3), 1.32 (m, 2H, $CH_2{}^e$), 1.22 (m, J_{PH} = 7.3, 7 Hz, 6H, CH_3), 1.01 (m, J_{PH} = 7.4, 7 Hz, 6H, CH_3); ^{31}P{^{1}H}: δ 96.6 (t, J_{PP} = 26 Hz), 84.4 (t, J_{PP} = 26 Hz).

Λ-[Ru((*S*,*S*)-Me-DuPHOS)$_2$(C_2H_4)], Λ-*S*,*S*-Ru2(η^2-C_2H_4) or Δ-[Ru-((*R*,*R*)-Me-DuPHOS)$_2$(C_2H_4)], Δ-*R*,*R*-Ru2(η^2-C_2H_4). The reaction proceeds in a similar manner to that for *R*,*R*-Me-BPE analogue with formation of the ethylene complex as single product. When the reaction is performed in hexane solution, the product precipitates as orange crystals. NMR (C_6D_6, 300 K), ^{1}H: δ 7.44 (d, J_{HH} = 6 Hz, 2H, Ph), 7.19 (d, J_{HH} = 7 Hz, 2H, Ph), 6.91 (quin, J_{HH} = 5 Hz, 4H, Ph), 2.61 (m, J_{HH} = 7 Hz, 2H, CH), 2.46 (m, J_{HH} = 7 Hz, 2H, CH), 2.04−1.74 (m, 12H, CH, CH_2, $CH_2{}^r$), 1.65 (q, J_{HH} = 8, J_{PH} = 7.3 Hz, 6H, CH_3), 1.59 (dd, J_{PH} = 7.4, J_{HH} = 7 Hz, 6H, CH_3), 1.50 (m, J_{HH} = 4, 12 Hz, 2H, $CH_2{}^e$), 1.27 (m, J_{HH} = 12, 4 Hz, 2H, $CH_2{}^e$), 0.30 (2 overlapping dd, J_{PH} = 7.4, J_{HH} = 7 Hz, 12H, $2CH_3$); ^{31}P{^{1}H}: δ 95.05 (t, J_{PP} = 30 Hz), 69.88 (t, J_{PP} = 30 Hz); ^{13}C{^{1}H}: δ 129.55 (t, J_{PC} = 7 Hz, CH^b), 128.57 (t, J_{PC} = 6 Hz, CH^b), 127.42, 125.82 (s, CH^b), 48.24 (t, J_{PC} = 12 Hz, CH), 43.65 (m, CH), 38.19, 37.37 (s, $CH_2{}^r$), 35.6 (m, CH), 34.3 (d, J_{PC} = 12 Hz, $CH_2{}^e$), 27.67 (m, CH), 21.9 (t, J_{PC} = 6 Hz, CH_3), 18.99 (t, J_{PC} = 7.4 Hz, CH_3), 18.74 (s, CH_3), 13.09 (s, CH_3). Anal. Calcd for $C_{38}H_{60}P_4Ru$ (741.81 g·mol^{-1}) C, 61.52; H, 8.15. Found: C, 61.14; H, 8.08. Mass spectra (EI, *m*/*z*): 714 (100%, $[M - C_2H_4]^+$).

Λ-[Ru((*R*,*R*)-Me-BPE)$_2$(CO)], Λ-*R*,*R*-Ru1(CO). An NMR tube was charged with Λ-*R*,*R*-Ru1H_2 (∼5 mg) and hexane; the solution was degassed, and CO (1 atm) was added. The color of the solution, upon irradiation with UV light, changed from colorless to slight yellow. The reaction is very slow compared to that of the DuPHOS analogue. Along with the formation of Ru(0), release of free phospholane and formation of minor byproduct is observed. NMR (C_6D_6, 300 K), ^{31}P{^{1}H}: δ 9.69 (br), 83.67 (br); (tol-d_8, 280 K), ^{31}P{^{1}H}: δ 104.52 (t, J_{PP} = 31 Hz), 88.06 (t, J_{PP} = 31 Hz). IR (toluene, cm^{-1}): 1606.

Δ-[Ru((*S*,*S*)-Me-DuPHOS)$_2$(CO)], Δ-*S*,*S*-Ru2(CO) or Λ-[Ru-((*R*,*R*)-Me-DuPHOS)$_2$(CO)], Λ-*R*,*R*-Ru2(CO). An NMR tube was charged with Λ-*R*,*R*-Ru2H_2 (∼ 5 mg) and hexane; the solution was degassed, and CO (1 atm) was added. The color of the solution, upon irradiation with UV light, changed from slightly yellow to intense red; the progress of the reaction was followed by ^{31}P NMR spectroscopy. NMR (C_6D_6, 300 K), ^{1}H: δ 7.79 (d, J_{HH} = 7 Hz, 2H, Ph), 7.39 (d, J_{HH} = 7 Hz, 2H, Ph), 7.18 (t, J_{HH} = 7 Hz, 2H, Ph), 7.11 (t, J_{HH} = 7 Hz, 2H, Ph), 2.96 (br m, J_{HH} = 7 Hz, 2H, CH_2), 2.63 (br m, J_{HH} = 7 Hz, 2H, CH_2), 2.37 (sept, J_{HH} = 7 Hz, 2H, CH), 2.27 (m, J_{HH} = 7 Hz, 2H, CH), 2.06 (m, J_{HH} = 7 Hz, 6H, CH, CH_2), 1.90 (dq, J_{HH} = 7 Hz, 2H, CH), 1.78 (m, J_{HH} = 7 Hz, 2H, CH_2), 1.65 (dd, J_{PH} = 17, J_{HH} = 7 Hz, 6H, $2CH_3$), 1.50 (m, J_{HH} = 7 Hz, 2H, CH, CH_2), 1.25 (overlapping dd, J_{PH} = 17, J_{HH} = 7 Hz, 12H, $4CH_3$), 0.47 (dd, J_{PH} = 17, J_{HH} = 7 Hz, 6H, $2CH_3$); ^{31}P{^{1}H}: δ 92.09 (t, J_{PP} = 35 Hz), 78.63 (t, J_{PP} = 35 Hz); ^{13}C{^{1}H}: δ 184.42 (m, C^{CO}), 151.58 (m, C^b), 147.61 (m, C^b), 132.05 (t, J_{PC} = 7 Hz, CH^b), 128.64 (t, J_{PC} = 8 Hz, CH^b), 128.50 (s, CH^b), 127.48 (s, CH^b), 50.53 (m, J_{PC} = 13 Hz, CH), 48.53 (m, J_{PC} = 6 Hz, CH), 39.71 (s, CH), 38.17 (t, J_{PC} = 16 Hz, CH), 36.59 (s, CH_2), 34.64 (s, CH_2), 20.17 (t, J_{PC} = 10 Hz, CH_3), 18.85 (t, J_{PC} = 5 Hz, CH_3), 14.76 (s, CH_3), 14.29 (s, CH_3). IR (toluene, cm^{-1}): 1872. Anal. Calcd for $C_{37}H_{56}OP_4Ru$ (742.23 g·mol^{-1}) C, 59.91; H, 7.61; O, 2.15. Found: C, 59.76; H, 7.61; O, 2.90. Mass spectra (LIFDI, *m*/*z*): 742 (100%, M^+), exp 742.2336, calcd for $C_{37}H_{56}OP_4Ru$ 742.2335, difference 1.1 mDa.

Λ-[*cis*-Ru((*R*,*R*)-Me-BPE)$_2$(Bpin)(H)], Λ-*R*,*R*-Ru1(Bpin)(H). An NMR tube was charged with Λ-*R*,*R*-Ru1H_2 (∼5 mg) and a slight excess of HBpin in hexane; the solution was degassed and then irradiated with UV light. The solution remains colorless. Progress of the reaction was followed by ^{31}P NMR spectroscopy. NMR (C_6D_6, 300 K), ^{1}H: δ 2.78 (m, J_{HH} = 7 Hz, 1H, CH_2), 2.66 (m, J_{HH} = 7 Hz, 1H, CH_2), 2.46 (m, J_{HH} = 6 Hz, 1H, CH_2), 2.16−1.87 (m, 15H, CH, CH_2, $CH_2{}^r$), 1.65 (m, 3H, CH, CH_2, $CH_2{}^r$), 1.55 (dd, J_{PH} = 7.6, J_{HH} = 7 Hz, 3H, CH_3), 1.48 (dd, J_{PH} = 7.8, J_{HH} = 7.6 Hz, 3H, CH_3), 1.39 (m, 2H, CH, CH_2, $CH_2{}^r$), 1.27 (m, 6H, CH_3), 1.18 (m, 3H, CH_3), 1.16 (s, 6H, BOC−CH_3), 1.15 (s, 6H, BOC−CH_3), 1.05 (dd, J_{PH} = 8, J_{HH} = 7.4 Hz, 3H, CH_3), 0.99 (dd, J_{PH} = 8, J_{HH} = 7.4 Hz, 6H, CH_3), 0.68 (m, 2H, CH_2), −9.85 (m, 1H, Ru−H); ^{31}P{^{1}H}: δ_A 110.2 (dt, J_{AX} = 237, J_{AM} = J_{AQ} = 16 Hz), δ_M 91.56 (q, J_{MA} = 16, J_{MQ} = J_{MX} = 18 Hz, P_{transH}), δ_Q 89.12 (br, P_{transB}), δ_X 88.1 (dt, J_{XA} = 237 Hz, J_{XM} = J_{XQ} = 18 Hz). ^{11}B δ 51 br. Mass spectra (LIFDI, *m*/*z*): 618 (100%, $[M - H_2]^+$), 746 (2%, M^+), exp 746.3400, calcd for $C_{34}H_{69}BO_2P_4Ru$ 746.3385, difference 1.5 mDa.

Δ-[*cis*-Ru((*S*,*S*)-Me-DuPHOS)$_2$(Bpin)(H)], Δ-*S*,*S*-Ru2(Bpin)(H) or Λ-[*cis*-Ru((*R*,*R*)-Me-DuPHOS)$_2$(Bpin)(H)], Λ-*R*,*R*-Ru2(Bpin)-(H). A similar procedure was followed resulting in a light yellow solution. NMR (C_6D_6, 300 K), ^{1}H: δ 7.75 (dd, J_{HH} = 7.7, J_{PH} = 7 Hz, 1H, Ph), 7.69 (t, J_{PH} = 12, J_{HH} = 7 Hz, 1H, Ph), 7.56 (d, J_{HH} = 7.5 Hz, 1H, Ph), 7.52 (m, J_{HH} = 7 Hz, 1H, Ph), 7.10 (m, J_{HH} = 7 Hz, 3H, Ph), 3.06 (m, J_{HH} = 6.8 Hz, 1H, CH_2), 2.96 (m, J_{HH} = 6 Hz, 2H, CH, CH_2), 2.76 (m, J_{HH} = 12, 5 Hz, 1H, CH), 2.58−2.51 (m, J_{HH} = 7, 4 Hz, 2H, CH, CH_2), 2.40 (m, 1H, CH), 2.29 (m, 4H, CH, CH_2), 2.10−1.77 (m, 8H, CH, CH_2), 1.62 (dd, J_{PH} = 18.6, J_{HH} = 7 Hz, 6H, $2CH_3$), 1.35 (dd, J_{HH} = 7 Hz, 6H, $2CH_3$), 1.17 (dd, J_{PH} = 12, J_{HH} = 7 Hz, 3H, CH_3), 0.82 (s, 12H, BOC−CH_3), 0.64 (dd, J_{PH} = 12, J_{HH} = 7 Hz, 12H, CH_3), −9.33 (m, 1H, Ru−H); ^{31}P{^{1}H}: δ_A 110.4 (dt, J_{AX} = 239, J_{AM} = J_{AQ} = 14 Hz), δ_X 93.03 (dt, J_{XA} = 239, J_{XM} = J_{XQ} = 19 Hz), δ_M 92.2 (m, overlapping with δ_X, J_{MA} = J_{MQ} = J_{MX} = 19 Hz, P_{transH}), δ_Q 82.47 (br, P_{transB}). ^{11}B δ 48.68 br. Mass Spectra (LIFDI, *m*/*z*): 714 (100%, $[M-H_2]^+$), 842 (10%, M^+), exp 842.3400, calcd for $C_{42}H_{69}BO_2P_4Ru$ 842.3385, difference 1.5 mDa.

trans-[Ru((*R*,*R*)-Me-DuPHOS)$_2$(C_6F_5)(H)], *trans*-*R*,*R*-Ru2(C_6F_5)-(H). A similar procedure was followed, resulting in a yellow solution containing a mixture of *trans*-*R*,*R*-Ru2(Br)(H) (resulting from impurities in pentafluorobenzene), starting material, and other minor products. Photolysis in neat C_6F_5H produced a small amount of precipitate, which was analyzed by NMR (C_6D_6, 300 K), ^{1}H: δ 7.66 (d, J_{HH} = 7 Hz, 2H, Ph), 7.50 (d, J_{HH} = 7 Hz, 2H, Ph), 7.23 (t, J_{HH} = 7 Hz, 2H, Ph), 2.93 (m, 2H, CH, CH_2), 2.60 (m, 1H, CH), 2.50 (m, 1H, CH, CH_2), 2.19 (m, 2H, CH), 1.93 (m, 5H, CH, CH_2), 1.74 (m, 3H, CH, CH_2), 1.47 (m, 3H, CH, CH_2), 1.27 (q, 6H, J_{PH} = 16, J_{HH} = 7 Hz, 6H, CH_3), 1.21 (q, 6H, J_{PH} = 16, J_{HH} = 7 Hz, 6H, CH_3), 0.81 (q, 6H, J_{PH} = 16, J_{HH} = 7 Hz, 6H, CH_3), 0.64 (q, 6H, J_{PH} = 17, J_{HH} = 7 Hz, 6H, CH_3), −13.14 (br m, 1H, Ru−H); ^{1}H{^{31}P}: δ −13.12 (br t, J_{FH} = 13 Hz, Ru−H); ^{31}P{^{1}H}: δ 85.98 (br), 84.41 (br); ^{19}F: δ −85.48 (m, 2F), −164.55 (m, 2F), −165.56 (t, J_{FH} = 13 Hz, 1F). Mass spectra (LIFDI, *m*/*z*): 882 (100%, M^+), exp 882.2399, calcd for $C_{42}H_{57}F_5P_4Ru$ 882.2374, difference 2.5 mDa.

■ ASSOCIATED CONTENT

Ⓢ Supporting Information

UV and CD spectra of precursors, photoproducts; NMR data including *trans* photoproducts; additional steady-state photolysis experiments; additional laser flash photolysis data; space filling models and additional crystallographic data; information

dx.doi.org/10.1021/ja210568t | J. Am. Chem. Soc. 2012, 134, 3480−3497

for all the crystal structures in CIF format. This material is available free of charge via the Internet at http://pubs.acs.org.

AUTHOR INFORMATION

Corresponding Author

robin.perutz@york.ac.uk

Notes

The authors declare no competing financial interest.

ACKNOWLEDGMENTS

We acknowledge the support of EPSRC. O.T. would like to thank the Ministerio de Ciencia e Innovación and the Fundación Española para la Ciencia y la Tecnología for funding. We thank Dr. Laurence Abbott, Dr. Richard Douthwaite, Prof. Simon Duckett, Dr. Sylviane Sabo-Etienne, and Dr. David Williamson for advice and assistance.

REFERENCES

(1) Meggers, E. *Eur. J. Inorg. Chem.* **2011**, 2911−2926.

(2) (a) Chmel, N. P.; Howson, S. E.; Allan, L. E. N.; Barker, J.; Clarkson, G. J.; Turner, S. S.; Scott, P. *Dalton Trans.* **2010**, *39*, 2919−2927. (b) Howson, S. E.; Scott, P. *Dalton Trans.* **2011**, *40*, 10268−10277.

(3) (a) Ziegler, M.; von Zelewsky, A. *Coord. Chem. Rev.* **1998**, *177*, 257−300. (b) Knof, U.; von Zelewsky, A. *Angew. Chem., Int. Ed.* **1999**, *38*, 302−322. (c) von Zelewsky, A.; Mamula, O. *J. Chem. Soc., Dalton Trans.* **2000**, 219−231.

(4) (a) Browne, W. R.; Hesek, D.; Gallagher, J. F.; O'Connor, C. M.; Killeen, J. S.; Aoki, F.; Ishida, H.; Inoue, Y.; Villani, C.; Vos, J. G. *Dalton Trans.* **2003**, 2597−2602. (b) Browne, W. R.; O'Connor, C. M.; Villani, C.; Vos, J. G. *Inorg. Chem.* **2001**, *40*, 5461−5464.

(5) (a) Oyler, K. D.; Coughlin, F. J.; Bernhard, S. *J. Am. Chem. Soc.* **2007**, *129*, 210−217. (b) Coughlin, F. J.; Oyler, K. D.; Pascal, R. A. Jr.; Bernhard, S. *Inorg. Chem.* **2008**, *47*, 974−979.

(6) Ashby, M. T.; Khan, M. A.; Halpern, J. *Organometallics* **1991**, *10*, 2011−2015.

(7) (a) Brunner, H. *Angew. Chem., Int. Ed.* **1999**, *38*, 1194−1208. (b) Brunner, H. *Eur. J. Inorg. Chem.* **2001**, 905−912. (c) Brunner, H.; Tsuno, T. *Acc. Chem. Res.* **2009**, *42*, 1501−1510. (d) Brunner, H.; Henning, F.; Weber, M. *Tetrahedron: Asymmetry* **2002**, *13*, 37−42. (e) Brunner, H.; Klankermayer, J.; Zabel, M. *Organometallics* **2002**, *21*, 5746−5756.

(8) (a) Albers, M. O.; Singleton, E.; Viney, M. M. *J. Mol. Catal.* **1985**, *33*, 77−82. (b) Saburi, M.; Ohnuki, M.; Ogasawa, M. T.; Takahashi, T.; Uchida, Y. *Tetrahedron Lett.* **1992**, *33*, 5783−5786.

(9) Câmpian, M. V.; Clot, E.; Eisenstein, O.; Helmstedt, U.; Jasim, N.; Perutz, R. N.; Whitwood, A. C.; Williamson, D. *J. Am. Chem. Soc.* **2008**, *130*, 4375−4385.

(10) Chen, Y.; Valentini, M.; Pregosin, P. S.; Albinati, A. *Inorg. Chim. Acta* **2002**, *327*, 4−14.

(11) (a) Cronin, L.; Nicasio, M.-C.; Perutz, R. N.; Peters, R. G.; Roddick, D. M.; Whittlesey, M. K. *J. Am. Chem. Soc.* **1995**, *117*, 10047−10054. (b) Nicasio, M. C.; Perutz, R. N.; Walton, P. W. *Organometallics* **1997**, *16*, 1410−1417. (c) Hall, C.; Jones, W. D.; Mawby, R. J.; Osman, R.; Perutz, R. N.; Whittlesey, M. K. *J. Am. Chem. Soc.* **1992**, *114*, 7425−7435. (d) Callaghan, P. L.; Fernández-Pacheco, R.; Jasim, N.; Lachaize, S.; Marder, T. B.; Perutz, R. N.; Rivalta, E.; Sabo-Etienne, S. *Chem. Commun.* **2004**, 242−243. (e) Perutz, R. N. *Chem. Soc. Rev.* **1993**, 361−369. (f) Montiel-Palma, V.; Perutz, R. N.; George, M. W.; Jina, O. S.; Sabo-Etienne, S. *Chem. Commun.* **2000**, 1175−1176. (g) Whittlesey, M. K.; Mawby, R. J.; Perutz, R. N.; Field, L. D.; Wilkinson, M. P.; George, M. W.; Osman, R. *J. Am. Chem. Soc.* **1993**, *115*, 8627−8637. (h) Nicasio, M.-C.; Perutz, R. N.; Tekkaya, A. *Organometallics* **1998**, *17*, 5557−5564. (i) Osman, R.; Pattison, D. I.; Perutz, R. N.; Bianchini, C.; Casares, J. A.; Peruzzini, M. *J. Am. Chem. Soc.* **1997**, *119*, 8459−8473.

(12) (a) Hartwig, J. F.; Andersen, R. A.; Bergman, R. G. *Organometallics* **1991**, *10*, 1710−1719. (b) Bergamini, P.; Sostero, S.; Traverso, O. *J. Organomet. Chem.* **1986**, *299*, C11−C14.

(13) (a) Colombo, M.; George, M. W.; Moore, J. N.; Pattison, D. I.; Perutz, R. N.; Virrels, I. G.; Ye, T.-Q. *J. Chem. Soc., Dalton Trans.* **1997**, 2857−2859. (b) Montiel-Palma, V.; Pattison, D. I.; Perutz, R. N.; Turner, C. *Organometallics* **2004**, *23*, 4034−4039. (c) Ampt, K. A. M.; Burling, S.; Donald, S. M. A.; Douglas, S.; Duckett, S. B.; Macgregor, S. A.; Perutz, R. N.; Whittlesey, M. K. *J. Am. Chem. Soc.* **2006**, *128*, 7452−7453. (d) Blazina, D.; Dunne, J. P.; Aiken, S.; Duckett, S. B.; Elkington, C.; McGrady, J. E.; Poli, R.; Walton, S. J.; Anwar, M. S.; Jones, J. A.; Carteret, H. A. *Dalton Trans.* **2006**, 2072−2080.

(14) (a) Macgregor, S. A.; Eisenstein, O.; Whittlesey, M. K.; Perutz, R. N. *J. Chem. Soc., Dalton Trans.* **1998**, 291−300. (b) Vendrelli, O.; Moreno, M.; Lluch, J. M. *J. Chem. Phys.* **2004**, *121*, 6258−6267.

(15) (a) Chan, V. S.; Stewart, I. C.; Bergman, R. G.; Toste, F. D. *J. Am. Chem. Soc.* **2006**, *128*, 2786−2787. (b) Chan, V. S.; Chiu, M.; Bergman, R. G.; Toste, F. D. *J. Am. Chem. Soc.* **2009**, *131*, 6021−6032.

(16) Schlaf, M.; Lough, A. J.; Morris, R. H. *Organometallics* **1997**, *16*, 1253−1259.

(17) Clark, G. R.; Falshaw, A.; Gainsford, G. J.; Lensink, C.; Slade, A. T.; Wright, L. J. *J. Coord. Chem.* **2010**, *63*, 373−393.

(18) (a) Burk, M. J.; Feaster, J. E.; Harlow, R. L. *Tetrahedron: Asymmetry* **1991**, *2*, 569−592. (b) Burk, M. J. *J. Am. Chem. Soc.* **1991**, *113*, 8518−8519. (c) Burk, M. J.; Feaster, J. E.; Nugent, W. A.; Harlow, R. L. *J. Am. Chem. Soc.* **1993**, *115*, 10125−10138.

(19) Nolan, S. P.; Belderrain, T. R.; Grubbs, R. H. *Organometallics* **1997**, *16*, 5569−5571.

(20) Budzelaar, P. H. M. gNMR, Version 5.0.6.0, IvorySoft, 2006.

(21) (a) Wiles, J. A.; Bergens, S. H.; Vanhessche, K. P. M.; Dobbs, D. A.; Rautenstrauch, V. *Angew. Chem., Int. Ed.* **2001**, *40*, 914−919. (b) Akotsi, O. M.; Metera, K.; Reid, R. D.; Mcdonald, R.; Bergens, S. H. *Chirality* **2000**, *12*, 514−522. (c) Moberg, V.; Homanen, P.; Selva, S.; Persson, R.; Haukka, M.; Pakkanen, T. A.; Monari, M.; Nordlander, E. *Dalton Trans.* **2006**, 279−288.

(22) In contrast to the corresponding reaction of Λ-*R*,*R*-Ru1H_2, a minor product is also formed in the reaction of Λ-*R*,*R*-Ru2H_2, with phenyl silane, due to the impurities present in the substrate.

(23) Tolman, C. A.; Ittel, S. D.; English, A. D.; Jesson, J. P. *J. Am. Chem. Soc.* **1978**, *100*, 4080−4089.

(24) Mkhalid, I. A. I.; Barnard, J. H.; Marder, T. B.; Murphy, J. M.; Hartwig, J. F. *Chem. Rev.* **2010**, *110*, 890−931.

(25) Irvine, G. J.; Lesley, G.; Marder, T. B.; Norman, N. C.; Rice, C. R.; Robins, E. G.; Roper, W. R.; Whittell, G. R.; Wright, J. *Chem. Rev.* **1998**, *98*, 2685−2722.

(26) (a) Clot, E.; Mégret, C.; Eisenstein, O.; Perutz, R. N. *J. Am. Chem. Soc.* **2009**, *131*, 7817−7827. (b) Clot, E.; Mégret, C.; Eisenstein, O.; Perutz, R. N. *J. Am. Chem. Soc.* **2006**, *128*, 8350−8357.

(27) Pertici, P.; Vitulli, G. *Inorg. Chim. Acta Lett.* **1979**, *37*, L521−L522.

(28) Dioumaev, V. K.; Procopio, L. J.; Carroll, P. J.; Berry, D. H. *J. Am. Chem. Soc.* **2003**, *125*, 8043−8058.

(29) Lachaize, S.; Sabo-Etienne, S. *Eur. J. Inorg. Chem.* **2006**, 2115−2127.

(30) (a) Lachaize, S.; Essalah, K.; Montiel-Palma, V.; Vendier, L.; Chaudret, B.; Barthelat, J.; Sabo-Etienne, S. *Organometallics* **2005**, *24*, 2935−2943. (b) Montiel-Palma, V.; Lumbierres, M.; Donnadieu, B.; Sabo-Etienne, S.; Chaudret, B. *J. Am. Chem. Soc.* **2002**, *124*, 5624−5625.

(31) Wong, W.-K.; Chiu, K. W.; Statler, J. A.; Wilkinson, G.; Motevalli, M.; Hursthouse, M. B. *Polyhedron* **1984**, *3*, 1255−1265.

(32) Whittlesey, M. K.; Perutz, R. N.; Moore, M. F. *Chem. Commun.* **1996**, 787−788.

(33) Reade, S. P.; Acton, A. L.; Mahon, M. F.; Martin, T. A.; Whittlesey, M. K. *Eur. J. Inorg. Chem.* **2009**, *13*, 1774−1785.

(34) (a) Calladine, J. A.; Torres, O.; Anstey, M.; Ball, G. E.; Bergman, R. G.; Curley, J.; Duckett, S. B.; George, M. W.; Gilson, A. I.; Lawes, D. J.; Perutz, R. N.; Sun, X.-Z.; Volhardt, P. C. *Chem. Sci.* **2010**, *1*, 622−630. (b) Duckett, S. B.; George, M. W.; Jina, O. S.; Matthews, S. L.;

Perutz, R. N.; Voung, K. Q. *Chem. Commun.* **2009**, 1401−1403. (c) Calladine, J. A.; Duckett, S. B.; George, M. W.; Matthews, S. L.; Perutz, R. N.; Torres, O.; Voung, K. Q. *J. Am. Chem. Soc.* **2011**, 2303−2310.
(35) (a) Aguilar, J. A.; Eliott, P. I. P.; Lopez-Serrano, J.; Adams, R. W.; Duckett, S. B. *Chem. Commun.* **2007**, 1183−1185. (b) Aguilar, J. A.; Adams, R. W.; Duckett, S. B.; Green, G. G. R.; Kandiah, R. *J. Magn. Reson.* **2011**, *208*, 49−57.
(36) (a) Duckett, S. B.; Eisenberg, R.; Goldman, A. S. *J. Chem. Soc., Chem. Commun.* **1993**, 1185−1187. (b) Eisenschmid, T. C.; McDonald, J.; Eisenberg, R. *J. Am. Chem. Soc.* **1989**, *111*, 7267−7269. (c) Duckett, S. B.; Newell, C. L.; Eisenberg, R. *J. Am. Chem. Soc.* **1993**, 1156−1157. (d) Barkemeyer, J.; Haake, M.; Bargon, J. *J. Am. Chem. Soc.* **1995**, *117*, 2927−2928.
(37) Wilhelm, E.; Battino, R. *Chem. Rev.* **1973**, *73*, 1−9.
(38) The error bars represent statistical 95% confidence limits derived from the measurements shown.
(39) (a) Sadowy, A. L.; Ferguson, M. J.; McDonald, R.; Tykwinski, R. R. *Organometallics* **2008**, *27*, 6321−6325. (b) Feliz, M.; Guillamón, E.; Llusar, R.; Vicent, C.; Stiriba, S.-E.; Pérez-Prieto, J.; Barberis, M. *Chem.—Eur. J.* **2006**, *12*, 1486−1492. (c) Lee, C.-T.; Chen, J.-D.; Chen-Yang, Y. W.; Liou, L.-S.; Wang, J.-C. *Polyhedron* **1997**, *16*, 473−479. (d) Algarra, A. G.; Basallote, M. G.; Fernandez-Trujillo, M. J.; Feliz, M.; Guillamon, E.; Llusar, R.; Sorribes, I.; Vicent, C. *Inorg. Chem.* **2010**, *49*, 5935−5942.
(40) (a) Duckett, S. B.; Wood, N. J. *Coord. Chem. Rev.* **2008**, 2278−2291. (b) Aime, S.; Gobetto, R.; Canet, D. *J. Am. Chem. Soc.* **1998**, *120*, 6770−6773. (c) Bargon, J.; Kandels, J.; Kating, P.; Thomas, A.; Woelk, K. *Tetrahedron Lett.* **1990**, *31*, 5721−5724.
(41) (a) Duckett, S. B.; Newell, C. L.; Eisenberg, R. *J. Am. Chem. Soc.* **1994**, *116*, 10548−10556; (b) *J. Am. Chem. Soc.* **1997**, *119*, 2068. (c) Natterer, J.; Bargon, J. *Prog. NMR Spectrosc.* **1997**, *31*, 293−315.
(42) Aime, S.; Dastru, W.; Gobetto, R.; Russo, A.; Viale, A.; Canet, D. *J. Phys. Chem. A* **1999**, *103*, 9702−9705.
(43) Millar, S. P.; Jang, M.; Lachicotte, R. J.; Eisenberg, R. *Inorg. Chim. Acta* **1998**, *270*, 363−375.
(44) (a) Perutz, R. N.; Sabo-Etienne, S. *Angew. Chem., Int. Ed. Engl.* **2007**, *46*, 2578−2592. (b) Sabo-Etienne, S.; Chaudret, B. *Coord. Chem. Rev.* **1998**, *178*, 381−407. (c) Gusev, D. G.; Vymenits, A. B.; Bakmutov, V. I. *Inorg. Chem.* **1992**, *31*, 2−4. (d) Pons, V.; Conway, S. L. J.; Green, M. L. H.; Green, J. C.; Herbert, B. J.; Heinekey, D. M. *Inorg. Chem.* **2004**, *43*, 3475−3483. (e) Grellier, M.; Vendier, L.; Chaudret, B.; Albinati, A.; Rizzato, S.; Mason, S.; Sabo-Etienne, S. *J. Am. Chem. Soc.* **2005**, *127*, 17592−17593. (f) Crabtree, R. H.; Luo, X.-L. *J. Am. Chem. Soc.* **1990**, *112*, 6912−6918.
(45) Gianini, M.; Forster, A.; Haag, P.; von Zelewsky, A.; Stoeckli-Evans, H. *Inorg. Chem.* **1996**, *35*, 4889−4895.
(46) Albers, M. O.; Ashworth, T. V.; Oosthuizen, E.; Singleton, E. *Inorg. Synth.* **1989**, *26*, 68−77.
(47) Blazina, D.; Duckett, S. B.; Halstead, T. K.; Kozak, C. M.; Taylor, R. J. K.; Anwar, M. S.; Jones, J. A.; Carteret, H. A. *Magn. Reson. Chem.* **2005**, *43*, 200−208.
(48) (a) Linden, H. B. *Eur. J. Mass Spectrom.* **2004**, *10*, 459−468. (b) Gross, J. H.; Nieth, N.; Linden, H. B.; Blumbach, U.; Richter, F. J.; Tauchert, M. E.; Tompers, R.; Hofmann, P. *Anal. Bioanal. Chem.* **2006**, *386*, 52−58.
(49) Stone, M. T.; Fox, J. M.; Moore, J. S. *Org. Lett.* **2004**, *6*, 3317−3320.
(50) Sheldrick, G. *Acta Crystallogr., Sect. A* **2008**, *64*, 112−122.
(51) Dolomanov, O. V.; Bourhis, J. L.; Gildea, R. J.; Howard, J. A. K.; Puschmann, H. OLEX2: a complete structure solution, refinement and analysis program. *J. Appl. Crystallogr.* **2009**, *42*, 339−341.